Journal of Medicinal Chemistry

Article

pubs.acs.org/jmc

Ligand Binding Stepwise Disrupts Water Network in Thrombin: Enthalpic and Entropic Changes Reveal Classical Hydrophobic Effect

Adam Biela, Frank Sielaff, Felix Terwesten, Andreas Heine, Torsten Steinmetzer, and Gerhard Klebe*

Department of Pharmaceutical Chemistry, Philipps University Marburg, Marbacher Weg 6, 35032 Marburg, Germany

Supporting Information

ABSTRACT: Well-ordered water molecules are displaced from thrombin's hydrophobic S3/4-pocket by P3-varied ligands (Gly, D-Ala, D-Val, D-Leu to D-Cha with increased hydrophobicity and steric requirement). Two series with 2-(aminomethyl)-5-chlorobenzylamide and 4-amidinobenzylamide at P1 were examined by ITC and crystallography. Although experiencing different interactions in S1, they display almost equal potency. For both scaffolds the terminal benzylsulfonyl substituent differs in binding, whereas the increasingly bulky P3-groups address S3/4 pocket similarly. Small substituents leave the solvation pattern unperturbed as found in the uncomplexed enzyme while increasingly larger ones stepwise displace the waters. Medium-sized groups show patterns with partially occupied waters. The overall 40-fold affinity enhancement correlates with water displacement and growing number of van der Waals contacts and is mainly attributed to favorable entropy. Both Gly derivatives deviate from the series and adopt different binding modes. Nonetheless, their thermodynamic signatures are virtually identical with the homologous D-Ala derivatives. Accordingly, unchanged thermodynamic profiles are no reliable indicator for conserved binding modes.

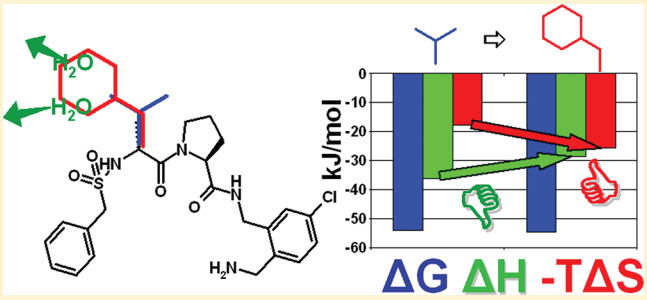

INTRODUCTION

Molecular recognition is of fundamental importance in biology and drug discovery. Especially in drug design, the demand for modulating the recognition features between a small molecule ligand and a target protein at will is of utmost importance as it provides an opportunity to interfere with a pathogenic mechanism where the target molecule plays a crucial role. Inhibition or enhancement of the activity of this target protein is one of the most popular approaches for the treatment of the associated disease. The binding process of a small ligand to a protein, no matter whether it results in inhibition or activation, is mediated, in the majority of cases, by noncovalent interactions. Hydrogen bonds, hydrophobic contacts, and charged interactions are in this context the most important interactions and they are believed to exert major part of binding affinity. Therefore, detailed understanding of the contributions of these types of interactions to the overall binding affinity is a prerequisite for the development of new and effective drugs against a target protein. In this respect, the accurate prediction of binding affinity of a drug candidate under consideration is pivotal to the idea of rational drug design. For example, how much does a newly formed hydrogen bond in a designed complex structure contribute to binding affinity, or is it virtually canceling out due to enthalpy/entropy compensation?[1−3] What is the role of water molecules in the binding event,[4,5] and how can we exploit hydrophobic interactions to achieve optimal ligand affinity?[6] These are only some questions which must be answered to put medicinal chemists in place to optimize their lead structures into potent drug candidates at will.[7] Our understanding of hydrophobic contributions to protein−ligand interactions is still rather rudimentary despite enormous research efforts which went into the characterization of the hydrophobic effect.[7] In its classical view, the hydrophobic effect experienced between interacting hydrophobic species is driven by the reorganization of water molecules upon protein−ligand binding.[8] Hydrophobic cavities in proteins and hydrophobic patches on ligand surfaces are exposed to water molecules prior to complex formation. These contacting water molecules are on first glance assumed to be well-ordered and thus associated with an unfavorable entropic component. According to textbook knowledge, the release of such water molecules from hydrophobic interfaces to the bulk water phase leads to a favorable entropic signal upon complex formation as the released water molecules gain additional degrees of freedom. The association of hydrophobic species is therefore assumed to be driven by an entropic enhancement. However, an impressive number of hydrophobic complex formations in biology and host−guest chemistry have been reported that follow an opposed enthalpy-driven thermodynamic profile and would thus intuitively contradict the classical view on the hydrophobic effect. Smithrud et al.,[9] for instance, tested the binding of benzene and pyrene derivatives to cyclophanes, and their results suggest a strongly exothermic signal upon complexation despite interaction of hydrophobic binding partners. The same could be observed for accommodating apolar molecules in the

Received: March 11, 2012
Published: May 21, 2012

dx.doi.org/10.1021/jm300337q | J. Med. Chem. 2012, 55, 6094−6110

cavity of cyclodextrins[10,11] and in the narrow AT-rich region of the DNA minor groove.[12,13] With respect to protein−ligand complex formation, examples were provided by Bingham et al.,[14] Englert et al.,[15] and Synder et al.[16] In the first case, binding of two pyrazine derivatives with propyl or butyl substituents to the hydrophobic binding pocket of the major urinary protein (MUP-1) was studied by ITC and resulted in an enthalpy-driven process. In the example of Englert et al., thermolysin was selected as model protein and its large hydrophobic S_1' pocket is addressed by ligand portions of gradually increasing size (methyl, propyl, isobutyl, and benzyl). The protein−ligand association was investigated by ITC and suggested also enthalpy-driven hydrophobic interactions. Notably, in both examined proteins, the binding pocket appears to be suboptimally hydrated[15,17] prior to ligand binding, and indeed, this common feature could explain the observed paradoxical enthalpic signal as proposed by Homans.[18] In a subsequent study, a deconvolution of the binding process in the MUP-1 case was done and it indicates that poor solvation of the uncomplexed pocket makes its desolvation even favorable. In other words, if a subsite is poorly solvated, only little enthalpy is required for its full desolvation in order to allow ligand binding. In the binding inventory, the unspent enthalpy pays off in an unexpectedly high enthalpy term as the released water molecules find enthalpically favorable interactions in the bulk water phase. These examples underline the importance of studying the solvation properties of hydrophobic ligands and hydrophobic protein pockets prior to complex formation to correctly consider their contributions to binding. This aspect is also decisive with respect to hydrophobic ligand optimization because addressing a poorly hydrated pocket could require a different design concept to enhance binding affinity than dealing with well-solvated pockets. In a recent study, Synder et al.[16] studied the thermodynamic profile of heterocyclic aromatic sulfonamides with increasing hydrophobic surface against carbonic anhydrase. Interestingly, they also received an enthalpy-driven signal with growing hydrophobicity. Here, the differences are explained by changes in the number and organization of well-ordered water molecules in the binding site. These studies clearly indicate that the thermodynamic signature of hydrophobic binding is determined by changes in the water structure and depend on the status of the water molecules being reorganized during the binding process. Also, from a computational point of view, the role of water in ligand binding and the factorization into enthalpic and entropic contributions has recently gained increasing appreciation.[19−26]

To shed some further light on this complex behavior, we investigated the occupancy of a rather well-solvated hydrophobic pocket to further characterize the driving forces for complex formation. We selected the large hydrophobic S3/4 pocket of thrombin as a model system and in contrast to the above-described examples, this pocket is well hydrated in uncomplexed state (PDB code 2UUF[25]). A feasible approach to evaluate the contributions from hydrophobic complex formation is to examine the influence of successive ligand structural variations on the binding thermodynamics. We systematically varied the P3 substituent of substrate−analogue peptidomimetics by incorporation of a Gly, D-Ala, D-Val, D-Leu, and a D-Cha to become increasingly more hydrophobic and sterically larger. To study these effects on broader scope, we synthesized two inhibitor series with different S1 occupants (see Table 1). 2-(Aminomethyl)-5-chlorobenzylamide (ACB)[26−29] and 4-amidinobenzylamide (AMBA)[30] are known anchors to bind with high potency to the S1 pocket. An experimental approach comprising ITC measurements, enzyme characterization, and high resolution crystal structure determination was applied to study the influence of a stepwise removal of water molecules from the hydrophobic S3/4 pocket of thrombin due to variations of the P3 residues.

Table 1. Chemical Structures of the Studied Ligands in the ACB and AMBA Series[b]

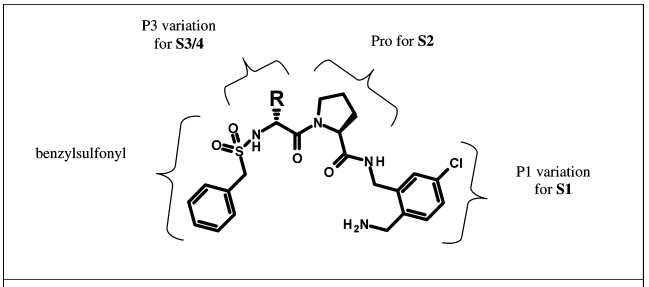

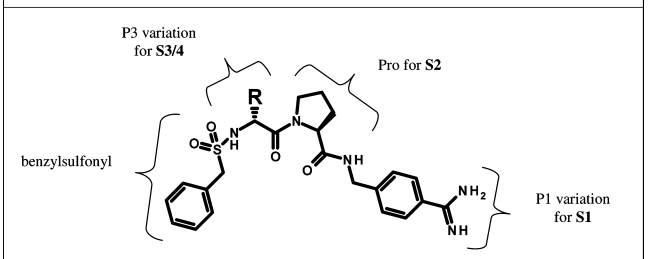

P1 substituent: ACB R:	K_i (nM)[a]	P1 substituent: AMBA R:	K_i (nM)[a]
1 H	1.5 ± 0.1	6 H	3.7 ± 0.6
2 CH_3	2.2 ± 0.4	7 CH_3	5.2 ± 0.8
3	0.798 ± 0.070	8	1.290 ± 0.347
4	0.259 ± 0.024	9	0.891 ± 0.115
5	0.052 ± 0.005	10	0.119 ± 0.010

[a]The estimated standard deviation of the K_i values is calculated from at least three measurements (in nM). [b]The designed variants R are given with the kinetically determined inhibition constants (K_i in nM) towards human thrombin.

RESULTS AND DISCUSSION

Crystal Structure Analysis. *Resolution Required for Interpreting Solvation Patterns.* To study systematically the replacement of water molecules from a binding pocket by crystallography requires high resolution crystal structures as the number of observed water molecules can depend on resolution of the diffraction data.[31] Statistics show that, on average, at 2.0 Å resolution, one water molecule per residue is included in the

dx.doi.org/10.1021/jm300337q | J. Med. Chem. 2012, 55, 6094−6110

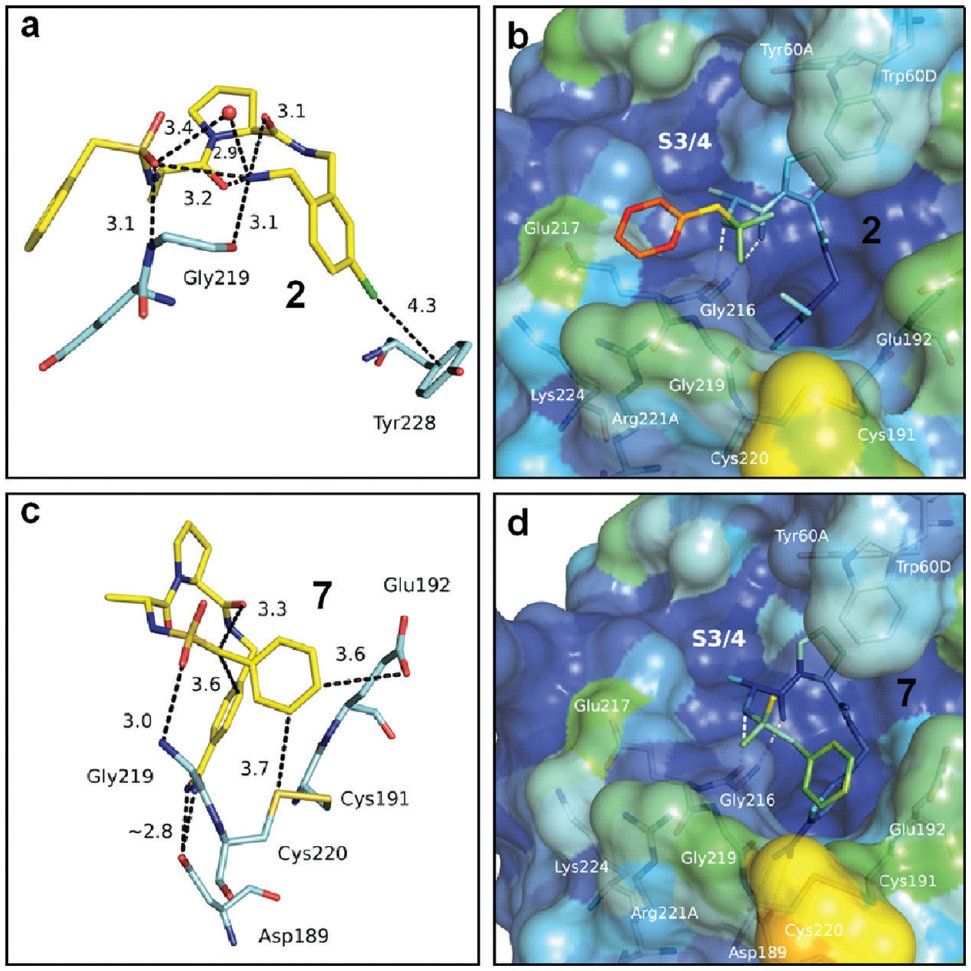

Figure 1. Binding modes of **2** and **7**. (a,c) The aminomethylene and the sulfonyl group in **2** are structurally organized by intramolecular H-bonds and an interstitial water molecule is picked up (a). For **7**, the interaction pattern near the disulfide bond is depicted in detail (c). Nitrogen is shown in blue, chlorine in green, sulfur in orange, oxygen in red, and carbon in yellow (ligand site) and cyan (protein site). Distances are given in Å. (b,d) Overall binding mode of **2** (b) and **7** (d) in complex with thrombin is shown with the protein's solvent-accessible surface. Colors are assigned to all atoms in (b) and (d) according to their temperature factors, from blue (low *B*-factor) to green and to red (high *B*-factor).

model, while at 1.0 Å resolution, about 1.6−1.7 are crystallographically located. We therefore used synchrotron radiation to achieve the best possible resolution of our complex structures. In total, 10 crystal structures of human thrombin in complex with **1**−**10** were determined with good to excellent resolution (1.78−1.23 Å).

*Binding Mode of the ACB Scaffold in **2**−**5**.* As the derivatives with a Gly P3 residue show completely different binding modes compared to the other members of the designed series, we will present their data in a separate section. The complex structures of **2**−**5** exhibit a comparable binding mode, and their binding will be exemplified using **2** as a representative (Figure 1a). The chlorine atom of the S1 occupant points toward the center of the Tyr228 ring with a distance of 4.3 Å suggesting a strong halogen−π interaction.[32] The aminomethylene anchor takes remarkable preorganizational influence on the overall binding mode. It is involved in intermolecular hydrogen bonds to the backbone carbonyl groups of Gly219 (3.1 Å) and Gly216 (3.1 Å). Furthermore, intramolecular contacts to (i) the oxygen atom of the inhibitor's own sulfonyl moiety (3.2 Å), (ii) the P2 (3.1 Å), and (iii) the P3 carbonyl groups (3.2 Å) are observed. This binding motif associates a water molecule that mediates an additional contact between both moieties. As we assume the primary amino group to be largely protonated at the applied pH 7.5, this interaction pattern is supposedly charge assisted. The pyrrolidine ring of proline is accommodated in the S2 pocket capped by Tyr60A and Trp60D of the 60s loop (Figure 1b). The methyl group of the P3-alanine is pointing into the S3/4 specificity pocket. The sulfonamide NH group and the adjacent central P3 carbonyl function form an antiparallel β-sheet-like binding motif to Gly216. This binding feature has already been observed in other inhibitor series, e.g., bearing a terminal amino group at this position.[33] One oxygen of the sulfonyl group is engaged in a hydrogen bond to the NH of Gly219 (3.1 Å) and, as mentioned, with the aminomethylene group of the P1 anchor (3.2 Å), while the other oxygen is pointing toward the bulk solvent. The intramolecularly preorganized binding geometry of this ligand series forces the terminal benzyl group to adopt an orientation that largely exposes this group to the bulk solvent without extensive hydrophobic contacts because it is mostly surrounded by hydrophilic amino acids (Arg221, Glu217, Lys224).

*Binding Mode of the AMBA Scaffold in **7**−**10**.* The scaffold of ligand **7** will be used to describe the binding features within the AMBA series. The AMBA anchor is placed into the S1 pocket to form a salt bridge with short distances (2.9 and 2.8 Å) to the deprotonated Asp189 at the bottom of this pocket

dx.doi.org/10.1021/jm300337q | *J. Med. Chem.* 2012, 55, 6094−6110

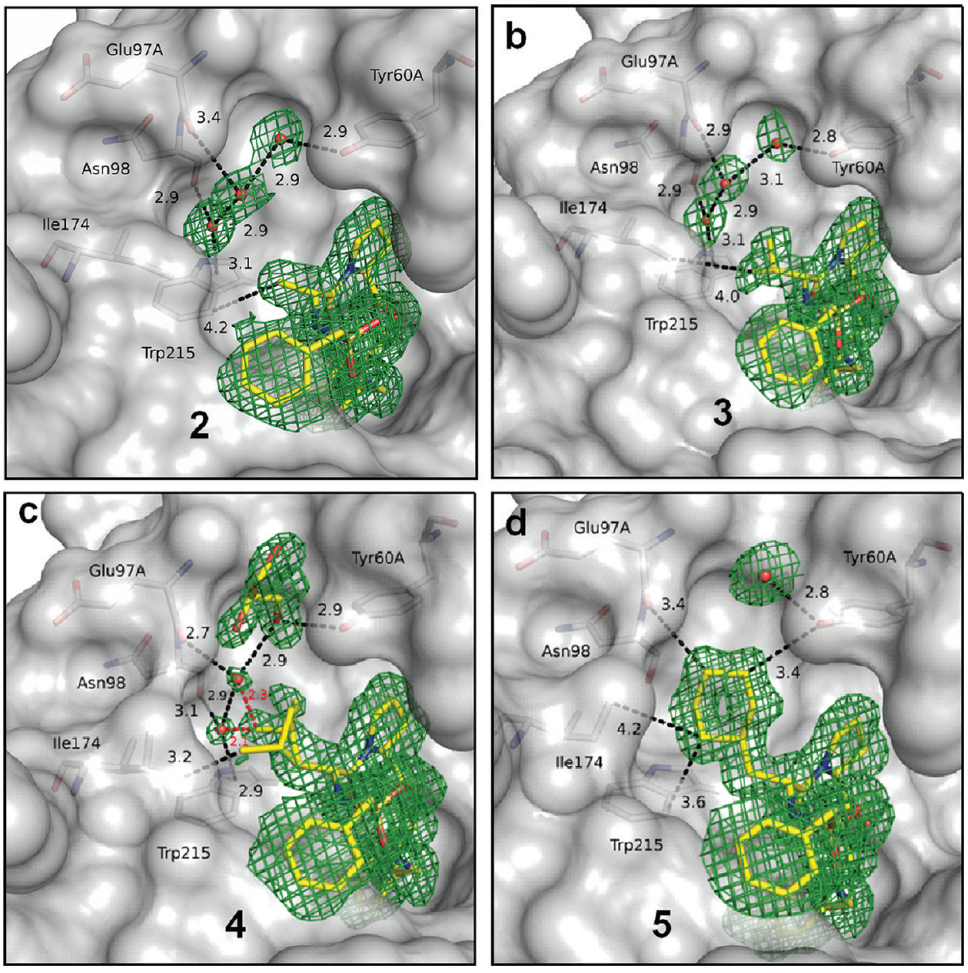

Figure 2. Binding modes of the ligands **2**−**5** with the ACB anchor group emphasizing the structural changes in the S3/4 region and in the ligand's P3 position. The $F_o - F_c$ difference electron density is shown as a green mesh at a 2σ level for **2** (a), **3** (b), **4** (c), and **5** (d) together with the bound water molecules in the S3/4 pocket if present. Favorable interactions with the corresponding distances in Å are depicted as broken lines. Values in red indicate short distances found for a specific contact described in the text. Nitrogen is shown in blue, chlorine in green, sulfur in orange, oxygen in red, and carbon in yellow (ligand site) and white (protein site); water molecules are given as red spheres.

(Figure 1c). The proline portion fits perfectly under the 60s loop of the S2 pocket, and the ligand's central amide NH and the adjacent carbonyl group form the above-mentioned β-ladder-type binding motif to the backbone of Gly216 with comparable distances (3.1 and 2.9 Å, Figure 1d). The sulfonyl takes a different role in this inhibitor series. It forms a short hydrogen bond (3.0 Å) to the backbone carbonyl of Gly219. In contrast to the ACB series, we could not observe any intramolecular hydrogen bonds in the AMBA examples. The lack of the aminomethylene anchor is most likely responsible for a different positioning of the terminal benzyl portion. It orients in opposite direction compared to the ACB series and binds to a shallow subpocket making a strong hydrophobic interaction to one of the sulfur atoms of the disulfide bridge between Cys220 and Cys191 (3.7 Å). A further van der Waals contact is found to the Cβ methylene and carboxyl group of Glu192 with a distance of 3.7 and 3.6 Å, respectively. Additionally, strong intramolecular hydrophobic contacts are observed between the terminal benzyl moiety and the phenyl ring of the AMBA (3.6 Å) and the inhibitor's own P2 carbonyl oxygen (3.3 Å). The U-shaped inhibitor conformation most likely results from a hydrophobic collapse. It is worth mentioning that the flexibility of the Glu192 side chain is strongly reduced in this complex, as the adjacent benzyl moiety restricts its accessible conformational space. Only one single Glu192 conformer is observed, whereas it is disordered in many other thrombin complexes.[34]

Crystallographic Analysis of Displaced Water Molecules and Implications on the Binding Affinity in the ACB Series ***2***−***5***. In the following, focus will be attributed to the displacement of water molecules from the S3/4 pocket. Ligand **2** with P3 D-Ala leaves the hydrophobic pocket well hydrated as the methyl group penetrates only slightly and does not reach the hydration shell (Figure 2a). The distance of the methyl group to the closest water molecule is 4.0 Å. Interestingly, the water network in this pocket shows remarkable features: The most deeply buried water molecule is bound to the backbone carbonyl of Asn98 (2.9 Å), and it is located on top of the center of the indole moiety of Trp215 (3.1 Å) to form a polar π-interaction.[35] The neighboring water molecule is rather loosely bound to the protein site (3.4 Å to Glu97A), and it is fixed in position by two flanking water molecules (2.9 Å each). The third water is located close to the rim of the pocket and interacts with the hydroxyl group of Tyr60A (2.9 Å). Besides one van der Waals contact to a carbon of Trp215 (4.2 Å), the P3-methyl group is not able to form any further interactions to the hydrophobic S3/4 pocket. Nevertheless, **2** exhibits a binding affinity of K_i = 2.2 ± 0.4 nM even though only weak

dx.doi.org/10.1021/jm300337q | J. Med. Chem. 2012, 55, 6094−6110

interactions with the pocket residues are experienced and no water displacement could be observed.

Replacement of the P3 methyl side chain in **2** by a larger isopropyl group in **3** changes the ligand's conformation little (Figure 3). Hardly any modifications of the solvation pattern of

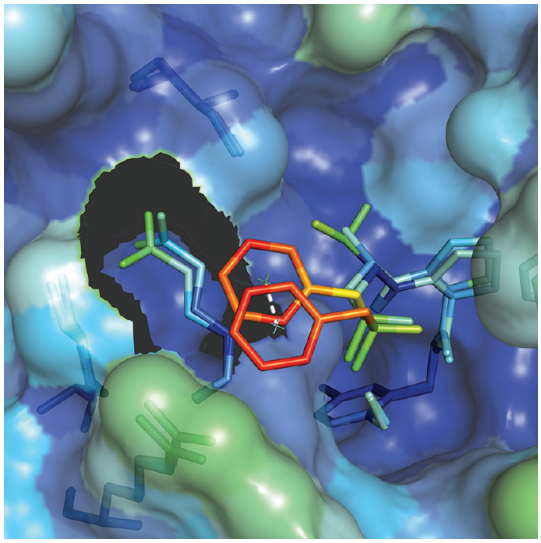

Figure 3. Superposition of ligands **2** and **3** to emphasize the shift of Glu217 and the movement of the benzyl portion in ligand **3**. Colors are assigned to all atoms according to their temperature factors, from blue (low *B*-factor) to green and to red (high *B*-factor). The solvent-accessible surface is shown. The distance indicated as broken line is given in Å.

the S3/4 pocket are apparent (Figure 2b). Obviously, the P3 D-Val seems to be too small to disrupt the S3/4 water network. The isopropyl group forms here a contact with CD1 of Ile174 (4.0 Å). Surprisingly, the isopropyl group does not point into the pocket but to the bulk solvent. This reorientation provokes a shift of the center of the terminal benzyl moiety by 1.5 Å compared to that in **2** (Figure 3). This movement is required to preserve a close contact between isopropyl group and benzyl moiety (now 3.9 Å). Furthermore, this slightly changed benzyl position induces the carboxyl group of Glu217 to adopt an orientation also found in the apo structure of thrombin, whereas in the complex with **2**, the carboxyl group is rotated by approximately 90° to allow binding of the benzyl portion (Figure 3). Compared to **2** no additional water molecule is displaced, the improved affinity (K_i = 0.788 ± 0.070 nM) by a factor of 3 might be related by the formation of two additional van der Waals contacts.

The D-Val/D-Leu exchange at P3 reveals some interesting binding features with disordered molecular portions both on protein and ligand side (see Figure 2c). The P3 isobutyl side chain could be refined in two orientations with conformation A (occupancy: 58%) inside and B (occupancy: 42%) outside the pocket. Conformation B induces a second orientation of Ile174 preventing too close contacts with the inhibitor.

Two populated water sites can be detected in the S3/4 pocket. They would be too close to conformation A (distance of 2.3 and 2.1 Å), and refinement of these water sites with full occupancy resulted in negative difference density (σ = −4.5). This encouraged us to refine these sites with partial occupancy as the water molecules can only be present in unit cells hosting conformation B.

Refinement of the latter water model with 42% occupancy revealed no remaining difference electron density. The observed disorder of the P3 D-Leu portion is therefore most likely correlated to the residual hydration of the S3/4 pocket. Despite the overall hydrophobic character of the S3/4 pocket, a perfect interaction network among the waters and to the protein is formed. As a matter of fact, a significant energetic price of desolvation has to be paid draining this well-hydrated subsite, which has to be compensated by the binding of **4**. Apparently, as a compromise, disorder is observed where in about half of the cases the S3/4 binding pocket remains solvated. Interestingly, in a previous contribution we showed a similar example with partial replacement of water molecules upon ligand binding in the S1 pocket of thrombin.[5] Subsumed, we suppose an average replacement of one water molecule from the S3/4 pocket upon binding of **4**. The kinetic measurement revealed a binding affinity of K_i = 0.259 ± 0.024 nM that is by a factor of 3 stronger than the affinity of the D-Val derivative **3** for which no water displacement has been observed.

The exchange of D-Leu by D-Cha in **5** showed significant changes of the S3/4 water network with displacement of two water molecules (Figure 2d). Only one water molecule at the border of the pocket is still retained, and it appears to be tightly bound to Tyr60A (2.8 Å). Detailed structural analysis shows remarkable van der Waals interactions between the cyclohexyl ring adopting chair conformation and the protein subsite. The contact distance to Trp215 is 3.6 Å and to Ile174 4.2 Å. Interestingly, we could not recognize two conformations for the side chain of Ile174 as observed with **4**. We assume a disfavored conformation as it is not observed in the apo structure and in complexes with **2** and **3**. Some close contacts (3.4 Å) are experienced by C−H vectors at the cyclohexyl ring and the carbonyl backbone of Glu97A or the hydroxyl group of Tyr60A. Most likely the displacement of two firmly bound water molecules and the extensive hydrophobic contacts to the P3 cyclohexyl side chain result in a further 5-fold improved affinity (K_i = 0.052 ± 0.005 nM) compared to **4**. The overall binding affinity was improved 42-fold from 2.2 nM for **2** to 0.052 nM for **5**.

*Crystallographic Analysis of the Displaced Water Molecules and Implications on the Binding Affinity in the AMBA Series **7**−**10**.* Using the AMBA series, we wanted to confirm the trends in the water displacement from the S3/4 pocket and study whether the different orientation of the terminal benzyl moiety takes any impact on the interaction pattern in the hydrophobic S3/4 pocket. Unfortunately, it turned out that the displacement of the water molecules could not be analyzed directly. Similarly to the ACB series, the AMBA-D-Ala derivative **7** orients its P3 methyl group into the S3/4 pocket. However, to our surprise, the remaining active site is filled by an additional inhibitor molecule showing 54% occupancy (Figure 4a). In this case, the benzylsulfonyl portion of the second ligand fits perfectly into the S3/4 pocket, resulting in its partial desolvation. In agreement with the partial occupancy of this second ligand, the diffraction data indicate at a position nearly coinciding with the benzyl moiety (1.3 Å), a density peak which suggests a partially occupied water molecule as a remainder of the above-described water network (Figure 5a). Occupancy of this water molecule was refined with 46% population, indicating its presence solely in absence of the second bound ligand. The hydrophobic portion of the second extra ligand exhibits pronounced van der Waals contacts (3.3−3.6 Å) with hydrophobic residues in the active site. Its sulfonyl group

dx.doi.org/10.1021/jm300337q | J. Med. Chem. 2012, 55, 6094−6110

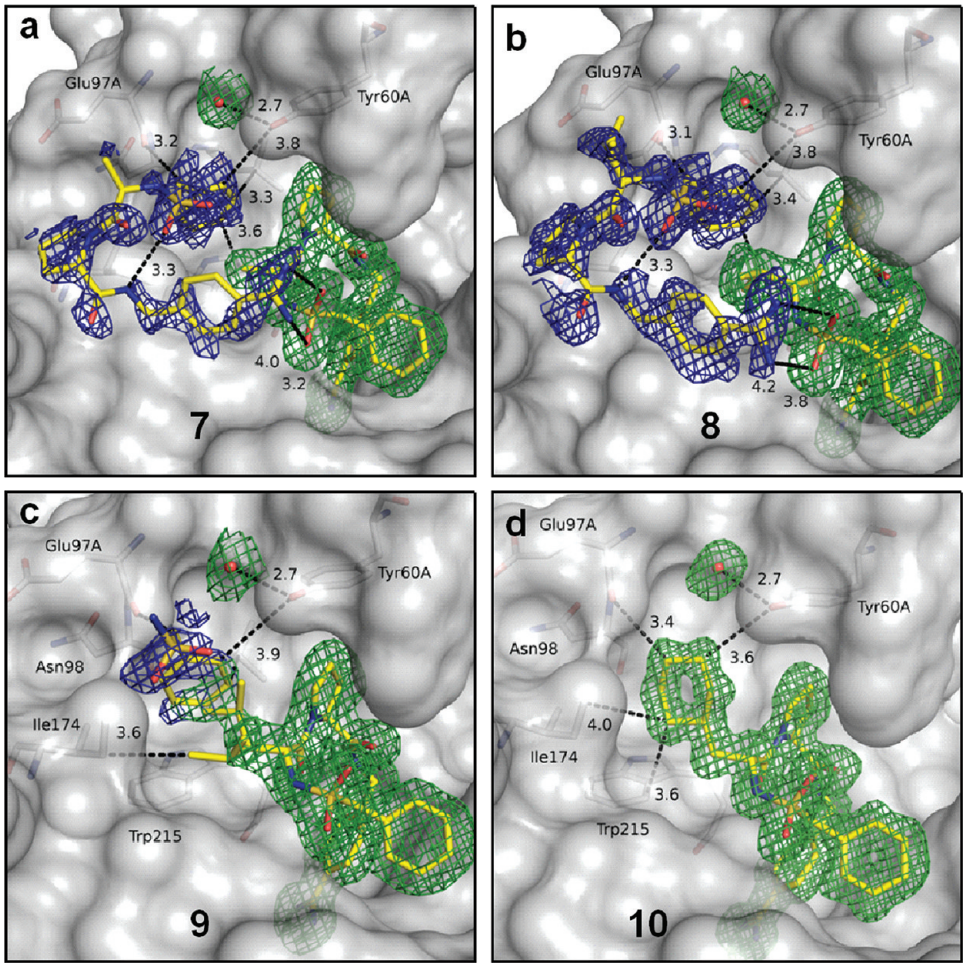

Figure 4. Binding modes of ligands **7**−**10** with the AMBA anchor group. Especially, the structural changes in the S3/4 region and in the ligand's P3 position are emphasized. The $F_o - F_c$ difference electron density is shown as a green mesh for the fully populated and in blue for the partially populated ligand at a 2σ level for **7** (a), **8** (b), **9** (c), and **10** (d) together with the bound water molecules in the S3/4 pocket if present. Favorable interactions with the corresponding distances in Å are depicted as broken lines.

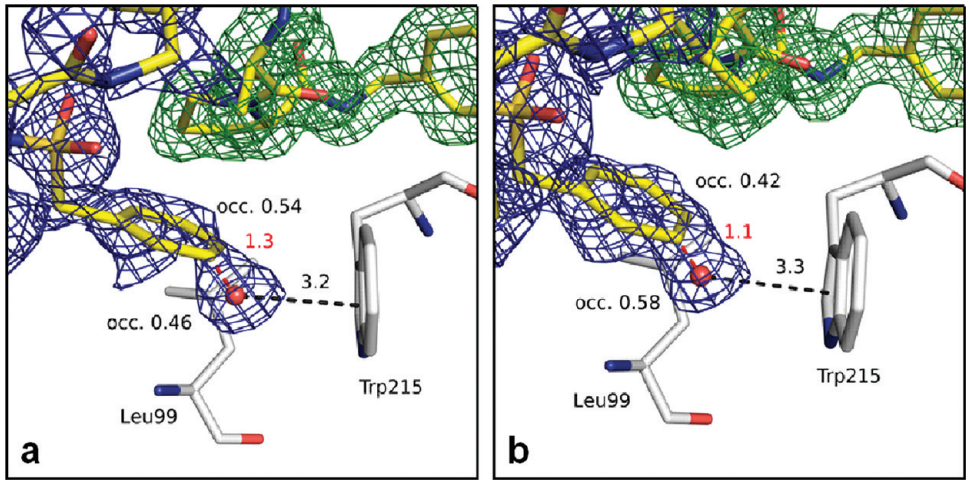

Figure 5. View from top on the S3/4 pocket to show close water contacts. The $F_o - F_c$ difference electron density is displayed as a green mesh for the fully populated and in blue for the partially populated ligand at a 2σ level for **7** (a) and **8** (b) together with the bound water molecule in the S3/4 pocket. Favorable interactions with the corresponding distances in Å are depicted as broken lines. Values in red indicate short distances in Å found for the specific atoms.

shows an intramolecular hydrogen bond (3.3 Å) to the NH group of its P2−P1 amide bond. The D-Ala and L-Pro portions are solvent-exposed with no notable interactions to the protein. The positively charged amidino function is weakly hydrogen bound (3.2 and 4.0 Å) to the sulfonyl part of the fully populated active-site bound ligand. The overall geometry

dx.doi.org/10.1021/jm300337q | J. Med. Chem. 2012, 55, 6094−6110

adopted by the extra ligand resembles also a U-shaped conformation. We checked whether any crystal packing effects could account for this unexpected crystallographic result. However, we could not detect any further hydrogen bonds to a symmetry-related protein molecule. The closest contact was found between the methyl group of the D-Ala portion and Glu13 of a neighboring crystal mate exhibiting rather large distance of 5.4 Å. Ligand **7** possesses comparable potency (K_i = 5.2 ± 0.8 nM) as the corresponding D-Ala derivative of the ACB series.

The D-Val derivative **8** shows the same properties again hosting two inhibitor molecules in the crystal structure with very similar binding poses (Figure 4b). The isopropyl group of the first fully populated active-site ligand points toward the S3/4 pocket. Also here the solvation pattern of this pocket is difficult to define due to the presence of a second extra inhibitor molecule with 42% occupancy. Nevertheless, the overlaid adjacent water site converged to 58% occupancy (Figure 5b). All contacts found for **8** compare well with those detected for **7**, whereas the binding affinity of **8** is increased by a factor of 3 to K_i = 0.788 ± 0.070 nM.

For the D-Leu derivative **9**, we observed an even more complex situation in the S3/4 pocket (Figure 4c). Again, two inhibitor molecules are found in the binding site. The first ligand is fully populated and well defined. The difference electron density suggests a very similar binding mode in agreement with the other series members. Differently, the electron density of the second extra-bound ligand is only poorly defined and we could solely include the benzylsulfonyl portion in our refinement model. The D-Leu side chain of the fully populated ligand **9** scatters over two conformations, each populated by 50%. The orientation outside the S3/4 pocket would allow binding of the second extra ligand forming the double hydrogen bond between the amidino group and the SO_2 group of the first molecule. Most likely, the orientation inside the pocket further reduces the occupancy of the extra ligand, resulting in its minor population. As a matter of fact, solely its benzylsulfonyl moiety could be assigned to the difference electron density. Inhibitor **9** has a slightly improved affinity likely due to its larger P3 residue (K_i = 0.891 ± 0.115 nM for **9**).

The cyclohexyl portion of **10** is large enough to fully occupy the S3/4 pocket. It completely disrupts the water network, concomitantly displacing two water molecules from the S3/4 pocket (Figure 4d). This ligand is found in the crystal structure with only one copy bound to the active site. As no space remains in the S3/4 pocket, no extra ligand binding is indicated. **10** proved to be the strongest binder in the AMBA series with an affinity of K_i = 0.119 ± 0.010 nM. The increasing hydrophobicity from methyl to cyclohexyl improved the affinity by a factor of 40. This is consistent with the first series. In general, the ACB inhibitors are always slightly more potent than the corresponding AMBA derivatives despite the lack of the salt bridge to Asp189, as seen in previous studies.[27]

*Comparison of the Binding Mode of the Second Additionally Bound Ligand in **7**–**9** to the Natural Substrate Fibrinogen of Thrombin.* Thrombin has a central role in blood coagulation. After activation from inactive prothrombin (II) to active thrombin (IIa), it converts soluble fibrinogen to insoluble fibrin which becomes cross-linked by factor XIIIa to form a stable clot.[36] Upon activation of the fibrinogen α-chain, the fibrinopeptide A (FPA), which is composed of 16 amino acids (^{1}ADSGEGDFLAEGGGVR^{16}), is cleaved off. Three crystal structures of human or bovine thrombin have been determined in complex with FPA or slightly modified analogues.[37−39] Superposition of both inhibitor molecules of **8** with a FPA-analogue (Figure 6) shows impressively that our bound ligands

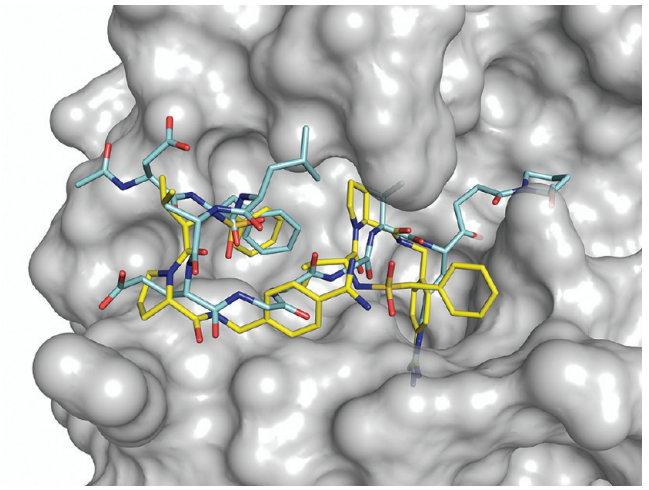

Figure 6. Active site region of thrombin in complex with the two bound ligand molcules of **8** and an FPA analogue (PDB code 1UCY[28]) containing a stable ketomethylene group (Argψ[CO-CH_2]Gly) instead of the scissile P1−P1′ peptide bond. The solvent-accessible surface of thrombin is depicted in gray. Nitrogen is shown in blue, sulfur in orange, oxygen in red, and carbon in yellow for ligand **8** and in cyan for the FPA derivative.

map well the binding geometry of FPA in complex with thrombin. In early days of thrombin research, it was a surprise that FPA binds with its P9 residue (Phe8) into the S3/4 pocket. It then leaves the cleavage site and forms a loop of six residues (Leu9-Gly14) to return with its P2 residue (Val15) into the S2 pocket. The second extra ligand in our study binds remarkably similarly with its benzyl portion into the S3/4 specificity pocket, as seen for the Phe8 side chain in FPA. It traces with its remaining scaffold the AEGG-loop of FPA that bulges out of the cleavage site.

*Crystal Structure Analysis of the Gly Derivatives **1** and **6**.* The Gly derivatives **1** and **6** of both series exhibit a different binding mode compared to the C_α substituted examples. For **1** and **6**, the geometry of the respective S1 occupants and the central proline are consistent with all other members of the series. Differences occur at P3 and involve the terminal benzylsulfonyl moiety. The latter hydrophobic portion is used to occupy the S3/4 pocket, which results in the displacement of two water molecules as similiarly observed for the cyclohexyl derivatives **5** and **10** (Figure 7a). The altered binding mode of **1** requires that the intramolecular water-mediated H-bond between the sulfonyl oxygen and the P1 aminomethylene anchor (present in **2**−**5**) is sacrificed and the interstitial water molecules are no longer detected. The aromatic ring of the terminal benzylsulfonyl moiety in **1** orients nearly perpendicular to the indole ring of Trp215 with a distance of 3.5 Å. Ile174 adopts a single conformation and rotates out of the pocket to avoid close contact with the benzyl moiety (3.8 Å). Both sulfonyl oxygens are exposed to the solvent. In spite of the displacement of two water molecules from the S3/4 pocket and remarkable van der Waals contacts, the Gly derivative **1** exhibits no significant gain in binding affinity (1.5 ± 0.1 nM) compared

dx.doi.org/10.1021/jm300337q | J. Med. Chem. 2012, 55, 6094−6110

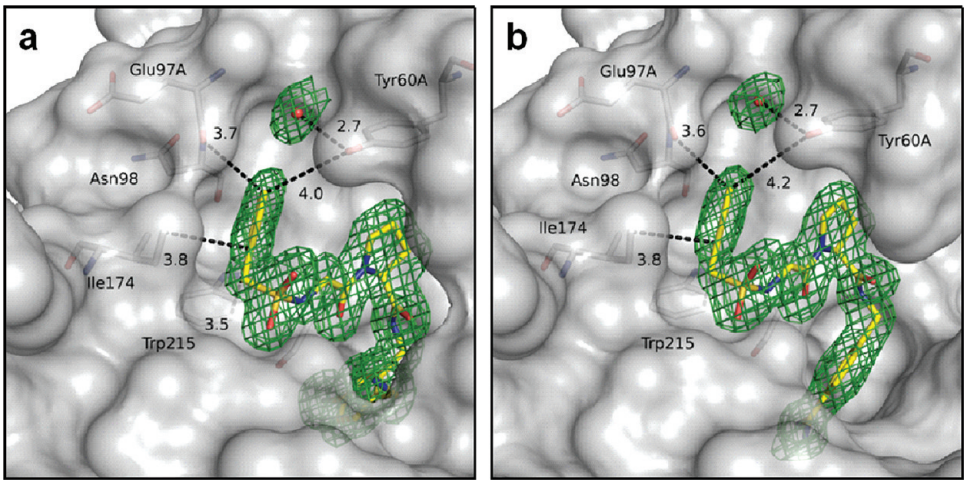

Figure 7. Binding mode of the glycine derivatives **1** (a) and **6** (b). The $F_o - F_c$ difference electron density is shown as a green mesh at a 2σ level. Favorable interactions with the corresponding distances in Å are depicted as broken lines.

to the D-Ala analogue **2** (2.2 ± 0.4 nM), where the pocket is completely solvated.

The AMBA analogue **6** adopts a comparable binding mode (Figure 7b). Again, its benzylsulfonyl portion is located in the S3/4 pocket and the sulfonyl oxygens are oriented toward the bulk solvent. Also, this ligand exhibits nearly the same affinity as the corresponding D-Ala analogue **7** (3.7 ± 0.6 nM and 5.2 ± 0.8 nM for **6** and **7**, respectively).

Thermodynamic Characterization. *Displacement Titration.* We used isothermal titration calorimetry (ITC) to determine the thermodynamic profiles of both series and to factorize Gibbs free energy of binding into enthalpic and entropic components. ITC is usually restricted to a range up to 5 nM using direct titrations. However, inhibitors investigated in this study show high potency from nano- to picomolar range. In such situations, direct measurement of tight binders is not possible, and we therefore applied displacement titrations to attain an accurate thermodynamic profile. Hence, the dissociation constant of the strong binder must be formally lowered to a range which can be recorded accurately by ITC.[40] In the displacement strategy, the protein solution is saturated by a "weak" binder such as **11** or **12** (Table 2). In the following step, the tight binder is titrated into the protein solution saturated with the first ligand (see Materials and Methods for details). During this titration, the "weak" binder is displaced by the strong one and the resulting sigmoidal titration curve can be analyzed according the displacement theory developed by Sigurskjold.[41]

Superimposed Proton Step. The measured heat signals showed dependence on the three buffers applied for the titrations (Table 3). This buffer dependence indicated protonation reactions superimposed onto the binding event. The net binding enthalpy can be extracted from these titrations by extrapolation (Figure 8). We observed comparable dependencies for all studied ligands suggesting a release of $n = 0.43 \pm 0.12$ mol protons upon binding (Figure 9). For a related series of ligands showing similar effects, Baum et al.[34] pointed out that His57 is responsible for the observed buffer dependency. As the functional groups in our ligands that could change protonation state (amidino group, aminomethylene group, sulfonamide group) are either too basic or very close to neutral pH, we anticipate that no ligand functional groups are involved in the protonation changes. Therefore, more likely, the imidazole moiety of His57 is partially protonated in the uncomplexed state and releases protons upon ligand accommodation.[42] After buffer correction, factorization of the Gibbs free energy shows increasingly entropy-driven binding which is consistent with the classical hydrophobic effect.

Table 2. Inhibitor Structures Used in the Displacement Titration As Competitive Binders Together with the Thermodynamically Determined Dissociation Contants (K_D in nM)[a] Towards Human Thrombin

Competitive Ligand 1 (**11**) 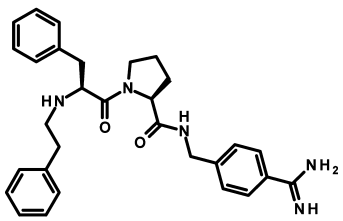	232 ± 48
Competitive Ligand 2 (**12**) 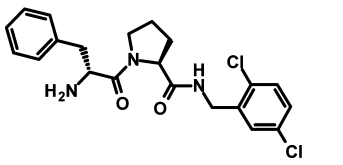	255 ± 16

[a]The estimated standard deviation of the K_D values is calculated from at least three measurements (in nM).

*Thermodynamic Profiles ACB series **2**–**5**.* The D-Ala derivative **2** reveals a thermodynamic profile that is clearly dominated by an enthalpic component ($\Delta H = -32.1$ kJ/mol for **2**). The entropic contribution amounts to about half of the enthalpy term ($-T\Delta S = -15.1$ kJ/mol for **2**). With growing size of the hydrophobic P3 substituent, we observed a constant increase of the entropic component and a slight decrease of the enthalpic signal. This thermodynamic signature is reversed from an enthalpy- to a more entropy-driven binding as larger hydrophobic portions are introduced at P3. Ligand **5**, with the largest hydrophobic portion, binds with a balanced thermodynamic profile, where both the enthalpy and entropy term, contribute almost equally to binding affinity ($\Delta H = -28.7$ kJ/mol and $-T\Delta S = -25.8$ kJ/mol for **5**). In our series, we

dx.doi.org/10.1021/jm300337q | J. Med. Chem. 2012, 55, 6094–6110

Table 3. Binding Data ΔG^0, ΔH^0, and $-T\Delta S^0$ (kJ/mol) of Ligands Determined by ITC

ligand name[a]	ΔG^0 (kJ/mol)	ΔH^0 (kJ/mol) in Tris[b]	ΔH^0 (kJ/mol) in tricine[b]	ΔH^0 (kJ/mol) in Hepes[b]	ΔH^0 (kJ/mol) buffer corrected	$-T\Delta S^0$ (kJ/mol)	no. of proton release (mol/mol)
1	−47.8 ± 0.1	−59.3 ± 1.3	−50.5	−46.1	**−35.4**	−12.4	0.49
2	−47.2 ± 0.9	−54.2 ± 0.6	−49.6	−40.9	**−32.1**	−15.1	0.48
3	−54.2 ± 0.2	−61.5 ± 0.7	−51.6	−47.7	**−36.2**	−18.0	0.52
4	−54.3 ± 1.4	−55.9 ± 1.9	−47.5	−41.3	**−30.1**	−24.2	0.54
5	−54.5 ± 0.1	−50.6 ± 0.1	−38.8	−39.8	**−28.7**	−25.8	0.43
6	−44.9 ± 1.1	−41.9 ± 0.1	−32.7	−26.3	**−14.3**	−30.6	0.58
7	−42.6 ± 0.2	−26.9 ± 0.5	−20.6	−21.6	**−15.9**	−26.7	0.21
8	−47.1 ± 0.1	−35.0 ± 1.0	−27.7	−23.1	**−13.8**	−33.3	0.44
9	−51.9 ± 1.0	−28.4 ± 2.3	−23.5	−17.9	**−10.4**	−41.5	0.38
10	−53.7 ± 0.8	−24.9 ± 0.1	−19.3	−17.7	**−11.4**	−42.3	0.27
11	−37.9 ± 0.5	−17.1 ± 1.1				−20.8 ± 1.7	
12	−37.6 ± 0.2	−37.5 ± 0.1				−0.1 ± 0.2	

[a]Inhibitors **1**−**10** were evaluated by displacement titrations using ligands **11** or **12** as competitive binder. The thermodynamic data of **11** and **12** were determined in a direct ITC titration in Tris buffer. [b]ΔH^0 was measured in three different buffers. Error ranges indicate the estimated standard deviations from at least duplicate measurements. Because the single point measurements in Hepes and tricine indicate a constant rate of proton release, these experiments were not performed in duplicate in order to save protein material (Figure 8).

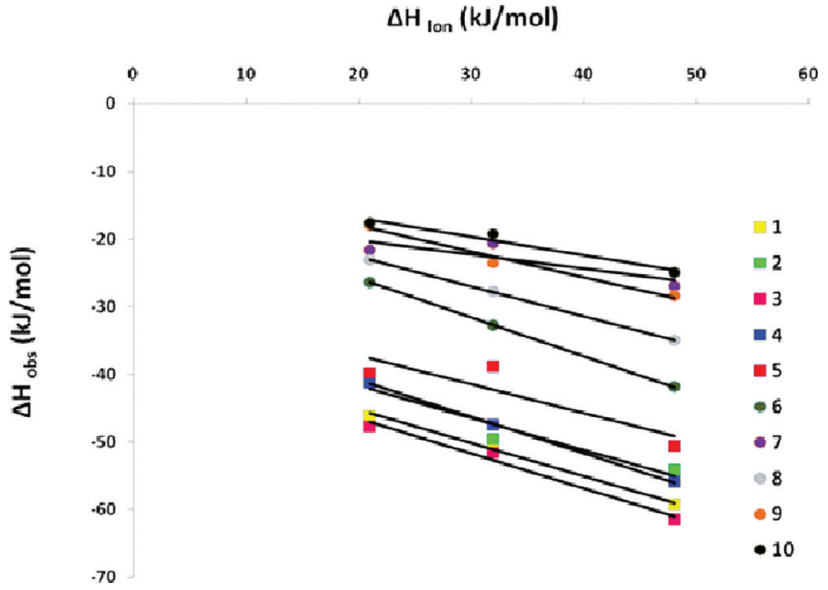

Figure 8. The measured heat signal is plotted against the ionization enthalpy of the buffer system (Tris, Hepes, and tricine) in order to extract the enthalpy of binding. The squares represent the values of the ligands from the ACB series (**1**−**5**) and the circles of the AMBA series (**6**−**10**).

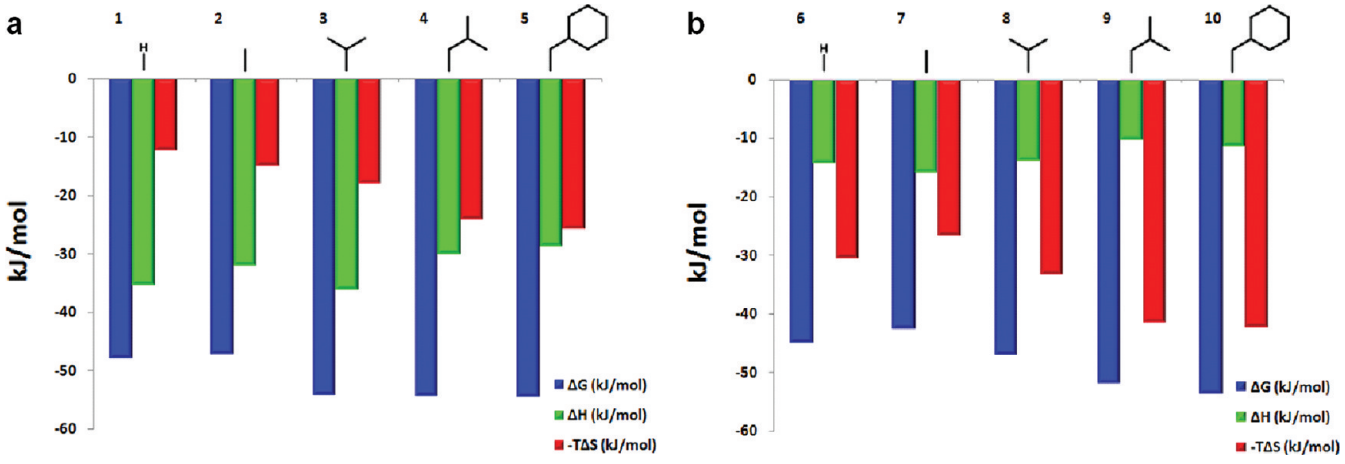

Figure 9. Thermodynamic parameters determined by ITC for ligands **1**−**5** (a) and **6**−**10** (b). The buffer corrected enthalpy values were used.

dx.doi.org/10.1021/jm300337q | J. Med. Chem. 2012, 55, 6094−6110

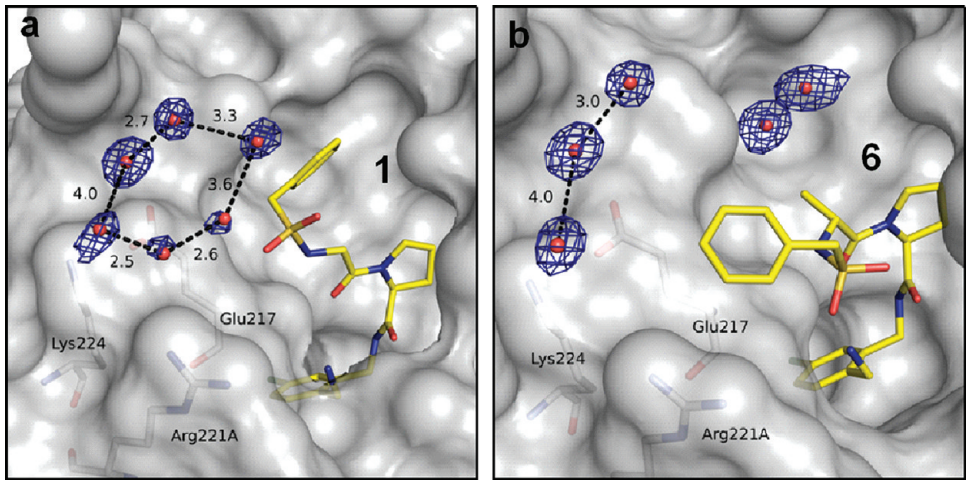

Figure 10. Binding mode of **1** (a) and **2** (b). The $2F_o - F_c$ difference electron density is contoured in blue at a 1σ level for the water molecules. Favorable interactions with the corresponding distances in Å are depicted as broken lines.

observe a slight overall decrease of enthalpy ($\Delta\Delta H_{2-5}$ = −3.4 kJ/mol), however, fortunately the entropy term overcompensates this enthalpy loss ($-T\Delta\Delta S_{2-5}$ = 10.7 kJ/mol). Therefore, a net gain in Gibbs free energy could be observed of $\Delta\Delta G_{2-5}$ = 7.3 kJ/mol.

*Thermodynamic Profiles AMBA Series **7**–**10**.* Comparable results are observed for the AMBA series, however, the thermodynamic signature starts from a different partitioning (Figure 9b). Here, the entropy term clearly governs the binding across the entire series (ΔH = −15.9 kJ/mol and $-T\Delta S$ = −26.7 kJ/mol for **7**) and it gradually increases from **7** to **10** during hydrophobic optimization, consistent with the findings in the ACB series. The entropic component of **10** is about four times the enthalpic signal (ΔH = −11.4 kJ/mol and $-T\Delta S$ = −42.3 kJ/mol for **10**), but the entropic enhancement is comparable to the ACB series. Again, we experience a net Gibbs free energy change of $\Delta\Delta G_{7-10}$ = 11.1 kJ/mol with a slight decrease in the enthalpic term ($\Delta\Delta H_{7-10}$ = −4.5 kJ/mol) outbalanced by a huge favorable entropic contribution ($-T\Delta\Delta S_{7-10}$ = 15.5 kJ/mol).

*Thermodynamic Profiles of the Gly Derivatives **1** and **6**.* The Gly derivatives **1** and **6** adopt quite different binding modes compared to the remaining examples of the two series. Surprisingly, this is *not* reflected in the thermodynamic profiles, as those for **1** and **6** fit quite reasonably into the series. Therefore, a closer comparison of the corresponding Gly and D-Ala derivatives should be regarded. Although **1** displaces two water molecules from the S3/4 pocket, we could only observe a slightly increased entropy component ($-T\Delta\Delta S_{1-2}$ = 2.7 kJ/mol) and basically no impact on the Gibbs free energy ($\Delta\Delta G_{1-2}$ = −0.6 kJ/mol) in comparison to **2**. As both ligands **1** and **2** position their benzyl moieties differently, we must examine whether a comparable displacement of water molecules occurs. **1** is able to desolvate the S3/4 pocket but leaves the adjacent hydrophilic site next to Glu217, Lys224, and Arg221 solvated (Figure 10a). In contrast, ligand **2** leaves the S3/4 pocket solvated but disrupts the solvation shell in the neighboring Glu217/Lys224/Arg221 region through accommodation of the benzyl portion (Figure 10b). Because of its polar character, the latter site is well solvated and the crystal structure of **1**, leaving this area unoccupied, does show here six bound water molecules, whereas in **2**, only three water molecules are present. Possibly the water replacement from the different subpockets results in a very similar thermodynamic signature for **1** and **2**. Furthermore, we observe a difference in the residual mobility of the benzyl portions of **1** and **2** which should also influence the entropic term. We analyzed the *B*-factor ratios of the benzyl portions relative to the remaining inhibitor molecules in order to estimate the degree of mobility. The benzylsulfonyl group of **1** exhibits low mobility [*B*(benzylsulfonyl)/*B*(P1 + P2 + P3) = 1.26] as it is tightly fixed in the S3/4 pocket, whereas in **2**, this portion shows substantially higher mobility [*B*(benzylsulfonyl)/*B*(P1 + P2 + P3) = 2.06]. This enhanced motion of the benzylsulfonyl portion is a common structural feature of **2**–**5** (1.90 for **3**, 1.69 for **4**, and 1.77 for **5**). The polar region next to Glu217/Lys224/Arg221A (Figure 3) is structured as a rather shallow crevice which is not suited to experience strong interactions with the benzyl portion. As a consequence, we observe this portion with pronounced residual mobility.

A similar situation is observed for **6** and **7**. Two water molecules are released to the bulk solvent by **6** but now with a slight entropic advantage ($-T\Delta\Delta S_{6-7}$ = −3.9 kJ/mol). This parallels a small loss in the free energy term ($\Delta\Delta G_{6-7}$ = −2.3 kJ/mol). Unfortunately, we cannot discuss here any details in hydration of the binding pockets (as done in **1**/**2**) as the extra bound ligand in the AMBA series prevents these insights. Surprisingly, the study of the *B*-factor ratios for the benzylsulfonyl portions reveals in this series equivalent values suggesting similar mobility [*B*(benzyl)/*B*(P1 + P2 + P3) = 1.58 for **6** and *B*(benzyl)/*B*(P1 + P2 + P3) = 1.51 for **7**]. All benzylsulfonyl moieties placed in this region next to the disulfide bridge reveal less mobility compared to the corresponding examples of the ACB series. It shows that the binding into the shallow subpocket in the vicinity to the disulfide bridge fixes the benzyl portion in **7** better than the polar environment of Glu217/Lys224/Arg221A in **2** (Figure 1b,d). This positioning of the benzyl is also known from inhibitor complexes with the related serine proteases factor Xa,[43] urokinase,[44] and factor VIIa.[45]

A further aspect affecting the partitioning of enthalpy and entropy of the Gly and D-Ala derivatives are the conformational differences in solution prior to protein binding. The Gly derivatives which lack an C_α substituent gain access to a larger conformational space in solution compared to the D-Ala examples. We studied the conformational behavior of these

dx.doi.org/10.1021/jm300337q | *J. Med. Chem.* 2012, 55, 6094–6110

ligand pairs by MD simulations in aqueous solution. The recorded angle distribution of Φ and Ψ next to the Gly and Ala residue clearly underscores the larger conformational multiplicity given for the Gly derivatives as it populates a broader range of torsion angles (cf. Figures S1 and S2, Supporting Information). As a consequence, this relates to a stronger loss in the conformational entropy of the Gly derivatives upon binding. Possibly, this entropic loss compensates to some extent the entropically beneficial water release from the formed complex and make the entropic signal less pronounced for **1** and **6**.

CONCLUSION

We performed a comprehensive study on water displacement upon binding of hydrophobic ligand portions to thrombin's well-hydrated S3/4 pocket. We studied the structural properties and thermodynamic signature driving the reorganization of the water structure. Several studies in literature showed that hydrophobic interactions are much more complex than generally believed, as in some examples the binding of hydrophobic species is accompanied with a clearly favorable enthalpy component instead of the expected entropy signal. As two studies[15,17] propose that a poorly defined hydration state of the protein pocket could be an explanation for an enthalpy-driven hydrophobic effect, we decided to address a hydrophobic pocket which is according to a high-resolution structure of uncomplexed thrombin well-hydrated and accessible to water molecules. Additionally, the study was performed with pico- to nanomolar ligands, which is in terms of thermodynamic characterization still a rather rarely explored field. The applied displacement titrations are elaborate as two titrations are necessary, but the results are reliable and well reproducible.

Two series with different S1 occupants were designed and synthesized which were systematically varied by hydrophobic residues (Gly, D-Ala, D-Val, D-Leu, and D-Cha) in the P3 position addressing the S3/4 pocket. In both series, the affinity improvement is correlated with the increasing size of the hydrophobic P3 side chain except for the Gly derivatives. The largest P3 substituent, D-Cha, shows highest affinity, whereas D-Ala in this position is in both series the weakest binder. The ACB series was optimized by a factor of 42, which is similar to the factor obtained in the AMBA series (40-fold).

As mentioned in the introduction, the ACB anchor is well-known to show high potency toward thrombin, but we found only two deposited thrombin complexes with this P1 group (PDB codes 1ZRB[29] and 3EQ0). These sparse structural data are quite surprising because the ACB portion is highly potent and less basic, which may lead to even better pharmacokinetic properties.[27] In our study, all ACB analogues possess slightly better binding affinity compared to the corresponding AMBA derivatives.

We observed a significant change in the binding mode of the P4-P3 segment moving from the Gly derivatives to C_α substituted examples. The Gly derivatives **1** and **6** occupy the S3/4 pocket and displace two water molecules, whereas the corresponding D-Ala analogues **2** and **7** do not penetrate into this pocket and leave it solvated. Surprisingly, no significant differences in the thermodynamic profile of corresponding Gly/Ala ligand pairs (**1**/**2**, **6**/**7**) are observed, indicating that unchanged thermodynamic signature is by no means a reliable indicator for conserved binding modes. The most likely experienced entropic benefit resulting from the displacement of two well-ordered water molecules from the S3/4 pocket by **1** and **6** is counterbalanced in the complexes of **2** and **7**. The latter ligands leave the S3/4 pocket solvated, but they desolvate another more polar site which remains hydrated in the complexes of **1** and **6**. Furthermore, differences in the residual mobility of the alternatively placed benzyl portions in **1**/**6** vs **2**/**7** influence the entropic profile as well as discrepancies in the accessible conformational space in solution prior to protein binding.

The structural investigation of the AMBA series revealed some surprising results. To the best of our knowledge, it is the first reported case where a small size peptidomimetic shows up twice as bound in and adjacent to the active site of thrombin. Superimposing the binding mode of both inhibitor skeletons with that of FPA, released from the natural substrate (Fibrinogen), reveals remarkable similarities in their recognition features. The soaking procedure was carried out at rather high inhibitor concentrations. Because we could not find evidence that the binding of the second extra ligands is significantly supported by crystal packing effects, possibly this additional binding mode could also be of some relevance in solution when working with high inhibitor concentration. Nevertheless, we assume the observed second bound molecule is of no relevance for enzyme inhibition under in vivo conditions, where plasma levels <1 μM are sufficient. Interestingly, it can provide a remarkable mapping of the substrate recognition area on the surface of the protease.

The thermodynamic characterization clearly suggests that the stepwise increase of the hydrophobic P3 substituent results in a growing potency which is associated with an enhanced entropic term. Both series start with the Gly/D-Ala derivatives having the smallest entropic contribution and end up with the cyclohexyl derivatives possessing a remarkably stronger entropic component. In this respect, our results support the current understanding of the classical hydrophobic effect being mainly entropy driven in nature and resulting from the release of firmly fixed water molecules from a well-hydrated binding pocket.

Remarkably, the AMBA series exhibits overall a stronger entropic binding component compared to the ACB series, even though for both series the growing size of the hydrophobic P3 substituent results in an increasingly entropic signature. What might be responsible for the stronger entropic profile of the AMBA series? In a previous study, we compared the properties of a benzamidine with *m*-chlorobenzyl P1 substituent.[33] In this analysis, the benzamidine portion is favored enthalpically by $\Delta\Delta H = -3.0$ kJ/mol and even more entropically by $-T\Delta\Delta S = -7.8$ kJ/mol compared to the *m*-chlorobenzyl group. As these P1 substituents are also present in the current series, a similar difference is given. Furthermore, the ACB series captures an interstitial water molecule upon binding which contributes to the enhanced enthalpic binding signal.[46] This fact also contributes to the larger enthalpic advantage of the ACB ligands.

MATERIALS AND METHODS

Synthesis. The detailed synthesis procedure for the D-Cha-inhibitors **5** and **10** was described recently.[47] The ACB analogues **2**−**4** were prepared according to the identical strategy as used for inhibitor **5** starting with the appropriate P4−P3 segments (Bzls-Gly-OH, Bzls-D-Ala-OH, Bzls-D-Val-OH, or Bzls-D-Leu-OH). These P4−P3 segments were alternatively coupled to H-Pro-4-amidinobenzylamide·2HCl[48] using PyBOP/diiodopropylethylamine in DMF, which provided the benzamidine derivatives **6**−**9**. All final inhibitors were purified by preparative reversed-phase HPLC to a purity >95% based at HPLC detection at 220 nm, as described previously.[49] The

dx.doi.org/10.1021/jm300337q | J. Med. Chem. 2012, 55, 6094−6110

Table 4. Data Collection and Refinement Statistics for the Thrombin Complex Structures 1−10

	THR-**1** complex (3RML)	THR-**2** complex (3RMM)	THR-**3** complex (3RMN)	THR-**4** complex (3T5F)	THR-**5** complex (3RMO)
(A) Data Collection and Processing					
no. crystals used	1	1	1	1	1
wavelength (Å)	1.00	1.00	0.91841	0.91841	1.00
space group	*C*2	*C*2	*C*2	*C*2	*C*2
unit cell parameters					
a, *b*, *c* (Å)	69.3, 71.2, 72.4	70.1, 71.1, 72.7	69.9, 71.1, 72.9	70.2, 71.0, 73.0	70.1, 71.0, 72.8
β (deg)	99.9	100.4	100.6	100.5	100.4
Matthews coefficient (Å^3/Da)	2.5	2.5	2.5	2.5	2.5
solvent content (%)	50	51	51	51	51
(B) Diffraction Data[a]					
resolution range (Å)	50−1.53 (1.56−1.53)	50−1.58 (1.61−1.58)	50−1.78 (1.81−1.78)	50−1.45 (1.48−1.45)	50−1.40 (1.42−1.40)
unique reflns	50478 (2436)	48248 (2403)	32972 (1610)	60276 (2698)	64957 (3195)
$R(I)$sym (%)	3.5 (35.7)	5.8 (47.8)	7.8 (47.6)	3.5 (33.9)	3.4 (37.0)
completeness (%)	96.4 (92.2)	99.8 (99.6)	97.9 (99.4)	96.5 (85.6)	94.0 (92.2)
redundancy	2.9 (2.7)	3.8 (3.7)	3.0 (2.9)	2.0 (2.0)	2.4 (2.4)
$I/\sigma(I)$	29.2 (2.7)	22.9 (3.0)	14.2 (2.1)	20.8 (2.2)	24.2 (2.2)
(C) Refinement					
resolution range (Å)	35.7−1.53	49.5−1.58	34.4−1.78	22.7−1.45	24.7−1.40
reflns used in refinement (work/free)	47916/2389	45959/2302	31209/1551	57070/875	61099/3089
final *R* values for all reflections (work/free) (%)	15.9/18.6	15.5/17.9	15.4/18.5	14.0/17.2	13.4/16.5
protein residues (L chain/H chain)	28/251	28/251	28/251	28/251	28/251
sodium ions	2	2	2	2	2
inhibitor atoms	32	33	35	36[b]/41[c]	39
water molecules	297	305	314	325	349
rmsd from ideality					
bond lengths (Å)	0.009	0.009	0.008	0.009	0.008
bond angles (deg)	1.08	1.08	1.06	1.04	1.05
Ramachandran plot					
residues in most favored regions (%)	85.8	85.0	85.8	86.2	85.0
residues in additionally allowed regions (%)	14.2	14.6	14.2	13.4	15.0
residues in generously allowed regions (%)	–	0.4	–	0.4	–
mean *B*-factor (Å^2)					
protein (L + H chain)	22.9	21.5	20.6	19.9	18.2
binding site[d]	18.5	16.7	15.8	16.2	14.8
inhibitor	17.5	21.0	18.5	22.4[e]	16.5
water molecules	33.6	33.7	32.5	32.5	36.0
	THR-**6** complex (3RLW)	THR-**7** complex (3RLY)	THR-**8** complex (3RM0)	THR-**9** complex (3UWJ)	THR-**10** complex (3RM2)
(A) Data Collection and Processing					
no. crystals used	1	1	1	1	1
wavelength (Å)	1.00	1.00	0.91841	0.91841	0.91841
space group	*C*2	*C*2	*C*2	*C*2	*C*2
unit cell parameters					
a, *b*, *c* (Å)	70.5, 71.3, 72.5	70.3, 71.4, 72.4	70.5, 71.3, 72.5	70.3, 71.2, 72.4	69.8, 71.5, 71.9
β (deg)	100.6	100.3	100.5	100.7	99.9
Matthews coefficient (Å^3/Da)	2.5	2.5	2.5	2.5	2.5
solvent content (%)	51	51	51	51	51
(B) Diffraction Data[a]					
resolution range (Å)	50−1.69 (1.72−1.69)	50−1.51 (1.54−1.51)	50−1.34 (1.36−1.34)	50−1.50 (1.53−1.50)	50−1.23 (1.25−1.23)
unique reflns	38822 (1961)	55139 (2742)	78347 (3850)	55148 (2816)	99085 (4675)
$R(I)$sym (%)	5.9 (49.0)	5.1 (48.7)	5.1 (51.9)	5.3 (46.8)	4.7 (38.7)

dx.doi.org/10.1021/jm300337q | *J. Med. Chem.* 2012, 55, 6094−6110

Table 4. continued

	THR-**6** complex (3RLW)	THR-**7** complex (3RLY)	THR-**8** complex (3RM0)	THR-**9** complex (3UWJ)	THR-**10** complex (3RM2)
(B) Diffraction Data[a]					
completeness (%)	97.7 (98.8)	99.9 (99.6)	98.7 (97.3)	97.3 (98.5)	97.9 (91.7)
redundancy	2.5 (2.4)	3.7 (3.5)	3.3 (3.3)	2.7 (2.6)	2.8 (2.1)
$I/\sigma(I)$	14.6 (2.0)	24.8 (2.7)	22.3 (2.2)	17.7 (1.9)	21.2 (2.0)
(C) Refinement					
resolution range (Å)	34.7−1.69	35.6−1.51	21.5−1.34	22.5−1.5	20.1−1.23
reflns used in refinement (work/free)	36443/1826	52718/2659	74108/3761	52016/2635	92538/4685
final *R* values for all reflections (work/free) (%)	16.2/19.2	15.5/17.2	14.0/16.6	16.0/18.3	14.0/16.3
protein residues (L chain/H chain)	28/251	28/251	28/251	28/251	28/251
sodium ions	2	2	2	2	2
inhibitor atoms	32	33[f]/33[g]	35[f]/35[g]	32[f]/11[g]	39
water molecules	243	347	361	349	390
rmsd from ideality					
bond lengths (Å)	0.008	0.009	0.008	0.018	0.008
bond angles (deg)	1.060	1.114	1.112	1.095	1.111
Ramachandran plot					
residues in most favored regions (%)	87.0	85.0	85.4	86.2	85.4
residues in additionally allowed regions (%)	13.0	15.0	14.6	13.8	14.6
residues in generously allowed regions (%)	–	–	–	–	–
mean *B*-factor (Å^2)					
protein (L + H chain)	22.9	19.1	18.0	17.7	17.4
binding site[b]	18.5	14.9	14.4	16.5	13.9
inhibitor	22.3	17.4[h]/26.7[i]	15.7[h]/16.9[i]	17.7[h]/21.1[i]	15.0
water molecules	31.4	32.4	31.5	33.6	33.3

[a]Numbers in parenthesis are for the highest resolution shell. [b]The inhibitor atoms from the additional disordered part were not considered. [c]All inhibitor atoms which were included in the refinement model. [d]Definition of the binding site: all amino acids which are 4 Å within the inhibitor. [e]Average *B* value for the ordered and fully ocupied inhibitor portion, the disordered portions were not considered. [f]Number of inhibitor atoms for the fully occupied ligand. [g]Number of inhibitor atoms for the partially occupied ligand. [h]Mean *B*-factor for the fully occupied ligand. [i]Mean *B*-factor for the partially occupied ligand.

analytical methods and data for inhibitors **1**−**10** are provided in the Supporting Information.

Bioassay. We characterized the potent inhibitors by a fluorogenic assay. Kinetic data were obtained using Tos-Gly-Pro-Arg-AMC[50] (tosyl-Gly-Pro-Arg-aminomethylcoumarin) as the fluorogenic substrate with a Safire II plate reader (Tecan, Switzerland, ex = 380 nm, em = 460 nm). This substrate allows us to work at a protein concentration of 0.050 nM, which is sufficiently lower than the lowest applied ligand concentration (0.780 nM). The experimental buffer contained 50 mM Tris-HCL, 154 mM NaCl, 0.1% polyethylene glycol 8000, and 5% DMSO at pH 7.4. The K_m of the substrate (1.1 ± 0.4 μM) was measured at 10 different substrate concentrations, and the resulting curve was analyzed using GraFit 4 software.[51] Cleavage of the substrate was measured by monitoring the change in fluorescence over a dilution series of at least 10 inhibitor concentrations (500−0.780 nM) at 5 μM substrate (S) over 600 s. The fluoroscence signal was plotted against time, and after linear regression the reaction rates (ν) were calculated. The latter values (ν) were plotted against the respective inhibitor concentration (I), and the resulting curve was fitted with ORIGIN software using equation 1. All measurements were performed at least in triplicate.

$$\nu = \frac{V_{max} \cdot S}{K_m \cdot \left(1 + \frac{I}{K_i}\right) + S} \quad (1)$$

Isothermal Titration Calorimetry. ITC experiments were performed using an ITC200 system from Microcal (now part of GE Healthcare, Northhampton, MA, USA). Thrombin Beriplast was freshly prepared for each experiment by dialysis of a thrombin sample in the buffer used for titration experiments (50 mM Tris, 100 mM NaCl, 0.1% polyethylene glycol 8000, 3% DMSO, pH 7.8). The ITC displacement experiment is composed of two titrations. The first experiment was done with one of the "weak-binding" ligands in a typical direct titration. For this purpose, after dialysis, the final **11** or **12** concentrations were achieved after dilution of the stock solution (40 mM, 100% DMSO) to the required ligand concentration (0.5 mM). The final DMSO concentration was subsequently adjusted to 3%. The reference cell contained pure water. The titration was started after the syringe was placed in the sample cell containing the thrombin solution (27 μM). The collected data were analyzed using ORIGIN Software (Microcal Inc.) by fitting a single-site-binding isotherm that yields ΔH^0 (enthalpy of binding) and K_D (dissociation constant). These data represent the thermodynamic profiles of the "weak-binding" ligands which are important for further analysis of the strong binders. After this first direct titration, the syringe was cleaned and filled with a solution of a strong binder (0.5 mM). The syringe was then placed into the sample cell which now contains the thrombin solution saturated with the "weak-binding" ligand from the first titration. During the titration, the strong ligand displaced step-by-step the "weak-binding" ligand from the binding pocket of thrombin. The experiment was stopped after small peaks of dilution indicated complete displacement of the "weak-binding" ligand from the binding site by the strong binder. The resulting curves were then analyzed using the competitive binding fitting function implemented in the ORIGIN software which was originally developed by Sigurskjold.[41] Each strong binder was characterized by this protocol by applying two

dx.doi.org/10.1021/jm300337q | J. Med. Chem. 2012, 55, 6094−6110

titrations in Tris buffer. These experiments were performed at least in duplicate.

ITC experiments in different buffers indicate a protonation reaction upon binding of the strong binders. The thermodynamic data were thus collected in addition to Tris buffer in 50 mM tricine and 50 mM Hepes buffer in a direct titration to achieve just the enthalpy component because these one point measurements indicate the expected constant rate of proton release. These experiments were not performed in duplicate in order to save protein material. The observed enthalpy values were plotted against the enthalpy of ionization of the applied buffer and fitted by linear regression to determine the intersection point with the y axis which represents the enthalpy of binding corrected by the buffer contribution (Figure 8).

All ITC experiments were started at 25 °C after a stable baseline had been achieved. The experimental design comprises an initial ligand injection of 0.3 μL followed by 15 injections of 1.1−1.4 μL with a 180 s interval between each injection.

Raw data were collected and the area under each peak was integrated, followed by correction for heats of dilution and mixing by subtracting the final baseline consisting of small peaks of the same size to zero. The initial data point was deleted from the integrated data because this injection usually reflects an erroneous amount of heat due to the possible exchange of liquids between syringe and cell when inserting the syringe into the calorimetric cell and the backlash error in the motorized screw mechanism in the injector.[52]

Crystallization and Soaking. Human α-thrombin (from Enzyme Research Laboratories, South Bend, IN, USA) was dissolved in the crystallization buffer (20 mM NaH_2PO_4, 350 mM NaCl, 2 mM benzamidine, pH 7.5) at 10 mg/mL. A hirudin fragment called acetyl-hirudin (54−65) purchased from Bachem (Bubendorf, Switzerland) was dissolved in crystallization buffer at 2.5 mg/mL. In the next step, 40 μL of the solution of the hirudin fragment was mixed with 160 μL of the thrombin solution. After incubation for 2 h at 4 °C, crystallization was carried out at 4 °C by the hanging-drop method. Then 1 μL of the hirudin/thrombin solution was placed in the center of a coverslip and mixed with 1 μL of reservoir solution (20 mM NaH_2PO_4, 27% polyethylene glycol 8000, pH 7.5). Immediately after the mixing of protein and reservoir buffer, microseeding was done. The wells of the crystallization trays were filled with 500 μL of the reservoir buffer. Subsequently, the coverslips were placed over the wells and sealed. Crystals of good diffracting quality were obtained after 7 days. For soaking, DMSO stock solutions of the inhibitors (50 mM) were diluted 1:10 with a solution containing 50% crystallization and 50% reservoir buffer, resulting in the final soaking concentration containing 5 mM of the inhibitor and 10% DMSO. Medium-size crystals without visible imperfections were selected and transferred into the soaking solution for 24 h.

Data Collection and Processing. Crystals were prepared for data collection at 110 K using a cryoprotectant solution of 20% glycerol in reservoir buffer. The data sets for **1**, **2**, **5**, **6**, and **7** were collected with synchrotron radiation at SLS (Villingen, Switzerland) on a Marmosaic 225 mm CCD detector. Complex structures for **3**, **4**, **8**, **9**, and **10** were collected at BESSY beamline 14.2 (Berlin, Germany) on a Rayonix MX 225 CCD detector. Data processing and scaling were performed using the HKL2000 package.[53]

Structure Determination and Refinement. The coordinates of human thrombin (PDB code 1H8D)[54] were used for initial rigid body refinement of the protein molecules followed by repeated cycles of maximum likelihood energy minimization, simulated annealing, and B-factor refinement using the CNS program package.[55] Structures **1**−**10** were refined with PHENIX.[56] The temperature factors for structures **5**, **8**, and **10** were anisotropically refined, whereas for structures **1**, **2**, **3**, **4**, **6**, **7**, and **9**, TLS refinement was applied. The definition of the TLS groups was done with the TLSMD server.[57,58] A randomly chosen 5% of all data were used for the calculation of R_{free} and were not used in the refinement. Amino acid side chains were fit into σ-weighted $2F_o - F_c$ and $F_o - F_c$ electron density maps using Coot.[59] After the first refinement cycle, water molecules and subsequently ions and ligands were located in the electron density and added to the model. Restraints were applied to bond lengths and angles, planarity of aromatic rings, and van der Waals contacts. Multiple side-chain conformations were built in case an appropriate electron density was observed and maintained during the refinement and if the minor populated side chain showed at least 20% occupancy. The final models were validated using PHENIX own validation options or MolProbity.[60] The Ramachandran plots were calculated with PROCHECK.[61] Data collection, unit cell parameters, and refinement statistics are given in Table 4. Analysis of temperature factors was done with Moleman[62] and fconv.[63] The naming of the protein amino acids was done according to Bode et al.[64] The figures were prepared using PyMOL 0.99. The Protein Data Bank accession codes of the coordinates and structure factors of all X-ray structures are given in Table 4.

Molecular Dynamics Simulations. The MD simulations were performed using AMBER 11[65] and Amber Tools 1.4. Extraction of the ligands from PDB files followed by the assignment of hydrogens was carried out using fconv.[63] Additional protonation of the amino group (**1**, **2**) and of the amidino group (**6**, **7**) was done using the program PyMOL.[66] After minimizing the ligands using the MMFF94x forcefield[67] implemented in the program MOE (version 2011.10), the preprocessed ligands were parametrized with the program antechamber using the generalized Amber force field (gaff).[68] Atomic charges were assigned by use of the AM1-BCC method.[69,70] Electroneutrality of the system was maintained by adding chloride ions as counterions followed by placing each starting structure in a truncated octahedral periodic box of TIP3P water molecules.[71] The closest distance between the edges of the water box and any distance of the solute was set to 10 Å. MD simulations were performed with pmemd.cuda under periodic boundary conditions using the particle mesh Ewald method[72] with a cutoff of 10 Å. The SHAKE algorithm[73] was applied to constrain bonds involving hydrogen. Langevin dynamics[74] with a predefined collision frequency of 5 ps^{-1} between external heat reservoir and simulated system were used to adjust temperature and isotropic position scaling to regulate pressure. The time steps of the simulation were set to 2 fs.

The water box was minimized by 100 cycles of steepest descent minimization followed by 400 cycles of conjugate gradient minimization. Afterward, the system consisting of water and ligand was minimized by 200 cycles of steepest descent minimization followed by 1000 cycles of conjugate gradient minimization. The system was gradually heated from 0 to 300 K in 150 ps using Cartesian restraints of 500 kcal mol^{-1} $Å^{-2}$ on the ligand followed by adjusting the pressure in 100 ps to 1 bar. Finally, before running the MD simulation, the restraints on the ligand were set gradually to 0 in 400 ps. The 100 ns MD simulation was performed storing the coordinates along the trajectory every 10 ps. Analysis of the trajectory was carried out using ptraj as implemented in Amber Tools 1.4.

■ ASSOCIATED CONTENT

Ⓢ Supporting Information

Additional experimental data concerning the synthesis. This material is available free of charge via the Internet at http://pubs.acs.org.

Accession Codes

Coordinates and structure factors have been deposited in the Protein Data Bank with the following accession codes: THR-**1** complex 3RML; THR-**2** complex 3RMM; THR-**3** complex 3RMN; THR-**4** complex 3T5F; THR-**5** complex 3RMO; THR-**6** complex 3RLW; THR-**7** complex 3RLY; THR-**8** complex 3RM0; THR-**9** complex 3UWJ; THR-**10** complex 3RM2.

■ AUTHOR INFORMATION

Corresponding Author

*Phone: +49 6421 282 1313. E-mail: klebe@mailer.uni-marburg.de.

Notes

The authors declare no competing financial interest.

■ ACKNOWLEDGMENTS

We kindly acknowledge CSL Behring, Marburg, for supplying us with generous amounts of human thrombin from the production of Beriplast. We thank the beamline support staff at SLS and BESSY for their advice during data collection. We acknowledge a travel grant from the Helmholtz Zentrum Berlin and the Swiss Light Source. We are grateful to Prof. David Hangauer and Maan Khayat (University at Buffalo, SUNY, New York, USA) for making a sample of compound **11** available to us. This work was supported by the Bundesministerium für Bildung und Forschung (BMBF, Förderkennzeichen 0315161C) and by the ERC grant 268145-DrugProfilBind kindly provided by EU.

■ ABBREVIATIONS USED

Cha, cyclohexylalanine; Bzls, benzylsulfonyl; PDB, Protein Data Bank; MD, molecular dynamics

■ REFERENCES

(1) Krishnamurthy, V. M.; Bohall, B. R.; Semetey, V.; Whitesides, G. M. The Paradoxical Thermodynamic Basis for the Interaction of Ethylene Glycol, Glycine, and Sarcosine Chains with Bovine Carbonic Anhydrase II: An Unexpected Manifestation of Enthalpy/Entropy Compensation. *J. Am. Chem. Soc.* **2006**, *128*, 5802−5812.

(2) Williams, D. H.; Stephens, E.; O'Brien, D. P.; Zhou, M. Understanding noncovalent interactions: ligand binding energy and catalytic efficiency from ligand-induced reductions in motion within receptors and enzymes. *Angew. Chem., Int. Ed.* **2004**, *43*, 6596−6616.

(3) Baum, B.; Muley, L.; Smolinski, M.; Heine, A.; Hangauer, D.; et al. Non-additivity of functional group contributions in protein-ligand binding: a comprehensive study by crystallography and isothermal titration calorimetry. *J. Mol. Biol.* **2010**, *397*, 1042−1054.

(4) Ladbury, J. E. Just add water! The effect of water on the specificity of protein−ligand binding sites and its potential application to drug design. *Chem Biol.* **1996**, *3*, 973−980.

(5) Biela, A.; Khyat, M.; Tan, H.; Heine, A.; Hangauer, D.; Klebe, G. Impact of ligand and protein desolvation on ligand binding to the S1 pocket of thrombin. *J. Mol. Biol.* **2012**, *418*, 350−366.

(6) Talhout, R.; Villa, A.; Mark, A. E.; Engberts, J. B. Understanding binding affinity: a combined isothermal titration calorimetry/molecular dynamics study of the binding of a series of hydrophobically modified benzamidinium chloride inhibitors to trypsin. *J. Am. Chem. Soc.* **2003**, *125*, 10570−10579.

(7) Whitesides, G. M.; Krishnamurthy, V. M. Designing ligands to bind proteins. *Q. Rev. Biophys.* **2005**, *38*, 385−395.

(8) Tanford, C. The hydrophobic effect and the organization of living matter. *Science* **1978**, *200*, 1012−1018.

(9) Smithrud, D. B.; Wyman, T. B.; Diederich, F. Enthalpically driven cyclophane−arene inclusion complexation: solvent-dependent calorimetric studies. *J. Am. Chem. Soc.* **1991**, *113*, 5420−5426.

(10) Eftink, M. R.; Harrison, J. C. Calorimetric studies of *p*-nitrophenol binding to α- and β-cyclodextrin. *Bioorg. Chem.* **1981**, *10*, 388−398.

(11) Bertrand, G. L.; Faulkner, J. R., Jr.; Han, S. M.; Armstrong, D. W. Substituent effects on the binding of phenols to cyclodextrins in aqueous solution. *J. Phys. Chem.* **1989**, *93*, 6863−6867.

(12) Breslauer, K. J.; Remeta, D. P.; Chou, W. Y.; Ferrante, R.; Curry, J.; Zaunczkowski, D.; Snyder, J. G.; Marky, L. A. Enthalpy−entropy compensations in drug−DNA binding studies. *Proc. Natl. Acad. Sci. U.S.A.* **1987**, *84*, 8922−8926.

(13) Marky, L. A.; Breslauer, K. J. Origins of netropsin binding affinity and specificity: correlations of thermodynamic and structural data. *Proc. Natl. Acad. Sci. U.S.A.* **1987**, *84*, 4359−4363.

(14) Bingham, R. J.; Findlay, J. B.; Hsieh, S. Y.; Kalverda, A. P.; Kjellberg, A.; Perazzolo, C.; Phillips, S. E.; Seshadri, K.; Trinh, C. H.; Turnbull, W. B.; Bodenhausen, G; Homans, S. W. Thermodynamics of binding of 2-methoxy-3-isopropylpyrazine and 2-methoxy-3-isobutylpyrazine to the major urinary protein. *J. Am. Chem. Soc.* **2004**, *126*, 1675−1681.

(15) Englert, L.; Biela, A.; Zayed, M.; Heine, A.; Hangauer, D.; Klebe, G. Displacement of disordered water molecules from hydrophobic pocket creates enthalpic signature: binding of phosphonamidate to the S_1'-pocket of thermolysin. *Biochim. Biophys. Acta* **2010**, *1800*, 1192−1202.

(16) Snyder, P. W.; Mecinovic, J.; Moustakas, D. T.; Thomas, S. W., III; Harder, M.; Mack, E. T.; Lockett, M. R.; Héroux, A.; Sherman, W.; Whitesides, G. M. Mechanism of the hydrophobic effect in the biomolecular recognition of arylsulfonamides by carbonic anhydrase. *Proc. Natl. Acad. Sci. U.S.A.* **2011**, *108*, 17889−17894.

(17) Barratt, E.; Bingham, R. J.; Warner, D. J.; Laughton, C. A.; Phillips, S. E.; Homans, S. W. Van der Waals interactions dominate ligand−protein association in a protein binding site occluded from solvent water. *J. Am. Chem. Soc.* **2005**, *127*, 11827−11834.

(18) Homans, S. W. Water, water everywhere—except where it matters? *Drug Discovery Today* **2007**, *12*, 534−539.

(19) Setny, P.; Baron, R.; McCammon, J. A. How Can Hydrophobic Association Be Enthalpy Driven? *J. Chem. Theory Comput.* **2010**, *6*, 2866−2871.

(20) Matysiak, S.; Debenedetti, P. G.; Rossky, P. J. Dissecting the Energetics of Hydrophobic Hydration of Polypeptides. *J. Phys. Chem. B* **2011**, *115*, 14859−14865.

(21) Wang, L.; Berne, B. J.; Friesner, R. A. Ligand binding to protein-binding pockets with wet and dry regions. *Proc. Natl. Acad. Sci. U.S.A.* **2011**, *108*, 1326−1330.

(22) Beuming, T.; Farid, R.; Sherman, W. High-energy water sites determine peptide binding affinity and specificity of PDZ domains. *Protein Sci.* **2009**, *18*, 1609−1619.

(23) Abel, R.; Salam, N. K.; Shelley, J.; Farid, R.; Friesner, R. A.; Sherman, W. Contribution of Explicit Solvent Effects to the Binding Affinity of Small-Molecule Inhibitors in Blood Coagulation Factor Serine Proteases. *ChemMedChem* **2011**, *6*, 1049−1106.

(24) Beuming, T.; Che, Y.; Abel, R.; Kim, B.; Shanmugasundaram, V.; Sherman, W. Thermodynamic analysis of water molecules at the surface of proteins and applications to binding site prediction and characterization. *Proteins: Struct., Funct., Bioinf.* **2012**, *80*, 871−883.

(25) Ahmed, H. U.; Blakeley, M. P.; Cianci, M.; Cruickshank, D. W. J.; Hubbard, J. A.; Helliwell, J. R. The determination of protonation states in proteins. *Acta Crystallogr., Sect. D: Biol. Crystallogr.* **2007**, *63*, 906−922.

(26) Rittle, K. E.; Barrow, J. C.; Cutrona, K. J.; Glass, K. L.; Krueger, J. A.; Kuo, L. C.; Lewis, S. D.; Lucas, B. J.; McMasters, D. R.; Morrissette, M. M.; Nantermet, P. G.; Newton, C. L.; Sanders, W. M.; Yan, Y.; Vacca, J. P.; Selnick, H. G. Unexpected enhancement of thrombin inhibitor potency with *o*-aminoalkylbenzylamides in the P1 position. *Bioorg. Med. Chem. Lett.* **2003**, *13*, 3477−3482.

(27) Dönnecke, D.; Schweinitz, A.; Stürzebecher, A.; Steinmetzer, P.; Schuster, M.; Stürzebecher, U.; Nicklisch, S.; Stürzebecher, J.; Steinmetzer, T. From selective substrate analogue factor Xa inhibitors to dual inhibitors of thrombin and factor Xa. Part 3. *Bioorg. Med. Chem. Lett.* **2007**, *17*, 3322−3329.

(28) Morrissette, M. M.; Stauffer, K. J.; Williams, P. D.; Lyle, T. A.; Vacca, J. P.; Krueger, J. A.; Lewis, S. D.; Lucas, B. J.; Wong, B. K.; White, R. B.; Miller-Stein, C.; Lyle, E. A.; Wallace, A. A.; Leonard, Y. M.; Welsh, D. C.; Lynch, J. J.; McMasters, D. R. Low molecular weight thrombin inhibitors with excellent potency, metabolic stability, and oral bioavailability. *Bioorg. Med. Chem. Lett.* **2004**, *14*, 4161−4164.

(29) Stauffer, K. J.; Williams, P. D.; Selnick, H. G.; Nantermet, P. G.; Newton, C. L.; Homnick, C. F.; Zrada, M. M.; Lewis, S. D.; Lucas, B. J.; Krueger, J. A.; Pietrak, B. L.; Lyle, E. A.; Singh, R.; Miller-Stein, C.; White, R. B.; Wong, B.; Wallace, A. A.; Sitko, G. R.; Cook, J. J.; Holahan, M. A.; Stranieri-Michener, M.; Leonard, Y. M.; Lynch, J. J., Jr.; McMasters, D. R.; Yan, Y. 9-hydroxyazafluorenes and their use in thrombin inhibitors. *J. Med. Chem.* **2005**, *48*, 2282−2293.

(30) Dullweber, F.; Stubbs, M. T.; Musil, D.; Stürzebecher, J.; Klebe, G. Factorising ligand affinity: a combined thermodynamic and

crystallographic study of trypsin and thrombin inhibition. *J. Mol. Biol.* **2001**, *313*, 593−614.
(31) Carugo, O.; Bordo, D. How many water molecules can be detected by protein crystallography? *Acta Crystallogr., Sect. D: Biol. Crystallogr.* **1999**, *55*, 479−483.
(32) Matter, H.; Nazaré, M.; Güssregen, S.; Will, D. W.; Schreuder, H.; Bauer, A.; Urmann, M.; Ritter, K.; Wagner, M.; Wehner, V. Evidence for C-Cl/C-Br···pi interactions as an important contribution to protein−ligand binding affinity. *Angew. Chem., Int. Ed. Engl.* **2009**, *48*, 2911−2916.
(33) Baum, B.; Mohamed, M.; Zayed, M.; Gerlach, C.; Heine, A.; Hangauer, D.; Klebe, G. More than a simple lipophilic contact: a detailed thermodynamic analysis of nonbasic residues in the S1 pocket of thrombin. *J. Mol. Biol.* **2009**, *390*, 56−69.
(34) Baum, B.; Muley, L.; Heine, A.; Smolinski, M.; Hangauer, D.; Klebe, G. Think twice: understanding the high potency of bis(phenyl)methane inhibitors of thrombin. *J. Mol. Biol.* **2009**, *391*, 552−564.
(35) Jain, A.; Ramanathan, V.; Sankararamakrishnan, R. Lone pair···pi interactions between water oxygens and aromatic residues: quantum chemical studies based on high-resolution protein structures and model compounds. *Protein Sci.* **2009**, *18*, 595−605.
(36) Hogg, D. H.; Blombäck, B. The mechanism of the fibrinogen−thrombin reaction. *Thromb. Res.* **1978**, *12*, 953−964.
(37) Martin, P. D.; Malkowski, M. G.; DiMaio, J.; Konishi, Y.; Ni, F.; Edwards, B. F. Bovine thrombin complexed with an uncleavable analog of residues 7−19 of fibrinogen A alpha: geometry of the catalytic triad and interactions of the P1′, P2′, and P3′ substrate residues. *Biochemistry* **1996**, *35*, 13030−13039.
(38) Stubbs, M. T.; Oschkinat, H.; Mayr, I.; Huber, R.; Angliker, H.; Stone, S. R.; Bode, W. The interaction of thrombin with fibrinogen. A structural basis for its specificity. *Eur. J. Biochem.* **1992**, *206*, 187−195.
(39) Martin, P. D.; Robertson, W.; Turk, D.; Huber, R.; Bode, W.; Edwards, B. F. The structure of residues 7−16 of the A alpha-chain of human fibrinogen bound to bovine thrombin at 2.3 Å resolution. *J. Biol. Chem.* **1992**, *267*, 7911−7920.
(40) Velazquez-Campoy, A.; Freire, E. Isothermal titration calorimetry to determine association constants for high-affinity ligands. *Nature Protoc.* **2006**, *1*, 186−191.
(41) Sigurskjold, B. W. Exact analysis of competition ligand binding by displacement isothermal titration calorimetry. *Anal. Biochem.* **2000**, *277*, 260−266.
(42) Czodrowski, P.; Sotriffer, C. A.; Klebe, G. Protonation changes upon ligand binding to trypsin and thrombin: structural interpretation based on pK_a calculations and ITC experiments. *J. Mol. Biol.* **2007**, *367*, 1347−1356.
(43) Schweinitz, A.; Stürzebecher, A.; Stürzebecher, U.; Schuster, O.; Stürzebecher, J.; Steinmetzer, T. New substrate analogue inhibitors of factor Xa containing 4-amidinobenzylamide as P1 residue: part 1. *Med. Chem.* **2006**, *2*, 349−361.
(44) Schweinitz, A.; Steinmetzer, T.; Banke, I. J.; Arlt, M. J.; Stürzebecher, A.; Schuster, O.; Geissler, A.; Giersiefen, H.; Zeslawska, E.; Jacob, U.; Krüger, A.; Stürzebecher, J. Design of novel and selective inhibitors of urokinase-type plasminogen activator with improved pharmacokinetic properties for use as antimetastatic agents. *J. Biol. Chem.* **2004**, *279*, 33613−33622.
(45) Shiraishi, T.; Kadono, S.; Haramura, M.; Kodama, H.; Ono, Y.; Iikura, H.; Esaki, T.; Koga, T.; Hattori, K.; Watanabe, Y.; Sakamoto, A.; Yoshihashi, K.; Kitazawa, T.; Esaki, K.; Ohta, M.; Sato, H.; Kozono, T. Factor VIIa inhibitors: target hopping in the serine protease family using X-ray structure determination. *Bioorg. Med. Chem. Lett.* **2008**, *18*, 4533−4537.
(46) Steuber, H.; Czodrowski, P.; Sotriffer, C. A.; Klebe, G. Tracing changes in protonation: a prerequisite to factorize thermodynamic data of inhibitor binding to aldose reductase. *J. Mol. Biol.* **2007**, *373*, 1305−1320.
(47) Sisay, M. T.; Steinmetzer, T.; Stirnberg, M.; Maurer, E.; Hammami, M.; Bajorath, J.; Gütschow, M. Identification of the first low-molecular-weight inhibitors of matriptase-2. *J. Med. Chem.* **2010**, *53*, 5523−5535.
(48) Steinmetzer, T.; Baum, B.; Biela, A.; Klebe, G.; Nowak, G.; Bucha, E. Beyond Heparinization: Design of highly potent thrombin inhibitors suitable for surface coupling. *ChemMedChem*, accepted, DOI: 10.1002/cmdc.201200292.
(49) Becker, G. L.; Sielaff, F.; Than, M. E.; Lindberg, I.; Routhier, S.; Day, R.; Lu, Y.; Garten, W.; Steinmetzer, T. Potent inhibitors of furin and furin-like proprotein convertases containing decarboxylated P1 arginine mimetics. *J. Med. Chem.* **2010**, *53*, 1067−1075.
(50) Bernett, M. J.; Blaber, S. I.; Scarisbrick, I. A.; Dhanarajan, P.; Thompson, S. M.; Blaber, M. Crystal structure and biochemical characterization of human kallikrein 6 reveals that a trypsin-like kallikrein is expressed in the central nervous system. *J. Biol. Chem.* **2002**, *277*, 24562−24570.
(51) Leatherbarrow, R. J. *GraFit Version 4*, 4.0 ed.; Erithacus Software Limited: Staines, UK, 1998.
(52) Mizoue, L. S.; Tellinghuisen, J. The role of backlash in the "first injection anomaly" in isothermal titration calorimetry. *Anal. Biochem.* **2004**, *326*, 125−127.
(53) Otwinowski, Z.; Minor, W. Processing of X-ray diffraction data collected in oscillation mode. *Methods Enzymol.* **1997**, *276*, 307−326.
(54) Skordalakes, E.; Dodson, G. G.; Green, D. S.; Goodwin, C. A.; Scully, M. F.; Hudson, H. R.; Kakkar, V. V.; Deadman, J. J. Inhibition of human alpha-thrombin by a phosphonate tripeptide proceeds via a metastable pentacoordinated phosphorus intermediate. *J. Mol. Biol.* **2001**, *311*, 549−555.
(55) Brunger, A. T.; Adams, P. D.; Clore, G. M.; DeLano, W. L.; Gros, P.; Grosse-Kunstleve, R. W.; Jiang, J. S.; Kuszewski, J.; Nilges, M.; Pannu, N. S.; Read, R. J.; Rice, L. M.; Simonson, T.; Warren, G. L. Crystallography & NMR system: a new software suite for macromolecular structure determination. *Acta Crystallogr., Sect. D: Biol. Crystallogr.* **1998**, *54*, 905−921.
(56) Adams, P. D.; Afonine, P. V.; Bunkóczi, G.; Chen, V. B.; Davis, I. W.; Echols, N.; Headd, J. J.; Hung, L. W.; Kapral, G. J.; Grosse-Kunstleve, R. W.; McCoy, A. J.; Moriarty, N. W.; Oeffner, R.; Read, R. J.; Richardson, D. C.; Richardson, J. S.; Terwilliger, T. C.; Zwart, P. H. PHENIX: a comprehensive Python-based system for macromolecular structure solution. *Acta Crystallogr., Sect. D: Biol. Crystallogr.* **2010**, *66*, 213−221.
(57) Painter, J.; Merritt, E. A. Optimal description of a protein structure in terms of multiple groups undergoing TLS motion. *Acta Crystallogr., Sect. D: Biol. Crystallogr.* **2006**, *62*, 439−450.
(58) Painter, J.; Merritt, E. A. TLSMD web server for the generation of multi-group TLS models. *J. Appl. Crystallogr.* **2006**, *39*, 109−111.
(59) Emsley, P.; Cowtan, K. Coot: model-building tools for molecular graphics. *Acta Crystallogr., Sect. D: Biol. Crystallogr.* **2004**, *60*, 2126−2132.
(60) Chen, V. B.; Arendall, W. B., III; Headd, J. J.; Keedy, D. A.; Immormino, R. M.; Kapral, G. J.; Murray, L. W.; Richardson, J. S.; Richardson, D. C. MolProbity: all-atom structure validation for macromolecular crystallography. *Acta Crystallogr., Sect. D: Biol. Crystallogr.* **2010**, *66*, 12−21.
(61) Laskowski, R. A.; MacArthur, M. W.; Moss, D. S.; Thornton, J. M. PROCHECK: a program to check the stereochemical quality of protein structures. *J. Appl. Crystallogr.* **1993**, *26*, 283−291.
(62) Kleywegt, G. J.; Zou, J. Y.; Kjeldgaard, M.; Jones, T. A. Around O. In *International Tables for Crystallography*; Rossmann, M. G., Arnold, E., Eds.; Kluwer Academic Publishers: Dordrecht, 2001; Vol. *F*, pp 353−356.
(63) Neudert, G.; Klebe, G. fconv: format conversion, manipulation and feature computation of molecular data. *Bioinformatics* **2001**, *27*, 1021−1022.
(64) Bode, W.; Mayr, I.; Baumann, U.; Huber, R.; Stone, S. R.; Hofsteenge, J. The refined 1.9 Å crystal structure of human alpha-thrombin: interaction with D-Phe-Pro-Arg chloro-methylketone and significance of the Tyr-Pro-Pro-Trp insertion segment. *EMBO J.* **1989**, *8*, 3467−3475.

(65) Case, D. A.; Darden, T. A.; Cheatham III, T. E.; Simmerling, C. L.; Wang, J.; Duke, R. E.; Luo, R.; Walker, R. C.; Zhang, W.; Merz, K. M.; Roberts, B. P.; Wang, B.; Hayik, S.; Roitberg, A.; Seabra, G.; Kolossváry, I.; Wong, K. F.; Paesani, F.; Vanicek, J.; Liu, J.; Wu, X.; Brozell, S. R.; Steinbrecher, T.; Gohlke, H.; Cai, Q.; Ye, X.; Wang, J.; Hsieh, M.-J.; Cui, G.; Roe, D. R.; Mathews, D. H.; Seetin, M. G.; Sagui, C.; Babin, V.; Luchko, T.; Gusarov, S.; Kovalenko, A.; Kollman, P. A. *AMBER 11*; University of California: San Francisco, 2010.
(66) *The PyMOL Molecular Graphics System*, version 1.2.x; Schrödinger LLC: New York.
(67) Halgren, T. A. Merck molecular forcefield. I. basis, form, scope, parameterization, and performance of MMFF94. *J. Comput. Chem.* **1996**, *17*, 490−519.
(68) Wang, J.; Wolf, R. M.; Caldwell, J. W.; Kollman, P. A.; Case, D. A. Development and testing of a general amber force field. *J. Comput. Chem.* **2004**, *25*, 1157−1174.
(69) Jakalian, A.; Bush, B. L.; Jack, D. B.; Bayly, C. I. Fast, efficient generation of high-quality atomic charges. AM1-BCC model: I. method. *J. Comput. Chem.* **2000**, *21*, 132−146.
(70) Jakalian, A.; Jack, D. B.; Bayly, C. I. Fast, efficient generation of high-quality atomic charges. AM1-BCC model: II. parameterization and validation. *J. Comput. Chem.* **2002**, *23*, 1623−1641.
(71) Jorgensen, W. L.; Chandrasekhar, J.; Madura, J. D.; Impey, R. W.; Klein, M. L. Comparison of simple potential functions for simulating liquid water. *J. Chem. Phys.* **1983**, *79*, 926−935.
(72) Darden, T.; York, D.; Pedersen, L. Particle mesh Ewald: An Nlog(N) method for Ewald sums in large systems. *J. Chem. Phys.* **1993**, *98*, 10089−10092.
(73) Ryckaert, J.-P.; Ciccotti, G.; Berendsen, H. J. C. Numerical integration of the cartesian equations of motion of a system with constraints: molecular dynamics of *n*-alkanes. *J. Comput. Phys.* **1977**, *23*, 327−341.
(74) Izaguirre, J. A.; Catarello, D. P.; Wozniak, J. M.; Skeel, R. D. Langevin stabilization of molecular dynamics. *J. Chem. Phys.* **2001**, *114*, 2090−2098.